Explanatory Supplement of the Mid-Infrared Spectrometer (MIRS) on board the Infrared Telescope in Space (IRTS)

(version 1.0)

(2003 February 26)

Takashi Onaka[a], Issei Yamamura[b], Thomas L. Roellig[c], Takafumi Ootsubo[a], Daisuke Ishihara[a], Kin-Wing Chan[a,c], Toshihiko Tanabè[d], and Martin Cohen[e]

[a]Department of Astronomy, School of Science, University of Tokyo, Tokyo 113-0033, Japan
[b]Institute of Space and Astronautical Science, Sagamihara, Kanagawa 229-8510, Japan
[c]NASA Ames Research Center, MS245-6, Moffett Field, CA94035-1000, U.S.A.
[d]Institute of Astronomy, School of Science, University of Tokyo, Tokyo 181-0015, Japan
[e]Radio Astronomy Laboratory, University of California, Berkeley, CA 94720, U.S.A.

Further author information: (Send correspondence to T. Onaka or T. L. Roellig) T.O.: E-mail: onaka@astron.s.u-tokyo.ac.jp; T.L.R.: Thomas.L.Roellig@nasa.gov. Present address of T. Ootsubo: National Astronomical Observatory, Japan, Mitaka, Tokyo 181-8588, Japan

1. INTRODUCTION

The Mid-Infrared Spectrometer (*MIRS*) is one of the four focal plane instruments on board the Infrared Telescope in Space (*IRTS*). The design and overview of the *IRTS* mission have been given in Refs. 1 and 2. The design of *MIRS* is described in Ref. 3. Here we will describe the latest status of the *MIRS* data reduction, including the flight performance, calibration, and point source extraction procedure of the *MIRS*.

2. INSTRUMENTATION AND FLIGHT OPERATION

In this section, we briefly describe the design and the flight operation of *MIRS*. Refer to Ref. 3 for details of the instrument design.

MIRS had 32 discrete Si:Bi photoconductor detectors. The output signals of the 32 detectors were multiplexed by two multiplexers in the cold stage and sent to the warm electronics. The signals were read by the integrating amplifiers. The amplifiers were automatically reset when the signal of one of the two channels most sensitive to the zodiacal emission (#15: 7.765 μm and #16: 7.990 μm channels) became 75% of the maximum in ADU (16 bits). Each detector was read every 0.512 sec (2Hz mode) or 1.024 sec (1Hz mode) depending on the telemetry rate. In the first period of the observations the low rate (1Hz mode) was used occasionally, but in the later phase of the mission the data were read all in the 2Hz mode. The period of 0.512 sec corresponded to about $2'$ on the sky at the scan rate of the *IRTS*. Therefore for those areas observed at the low sampling rate the data had less spatial information. The sampling speed of each individual detector was 2 msec. Since the aperture size of *MIRS* was $8' \times 8'$, the difference in the signal acquisition timing of the detectors was negligible.

The *MIRS* optics consisted only of a concave grating and field mirrors. A schematic view of the *MIRS* optical layout is shown in Figure 1. The concave grating had varied spaced grooves to correct the astigmatic aberrations.[4] Because of the nature of the concave grating, the spectral resolution of *MIRS* is somewhat dependent on the wavelength (see section 3.4).

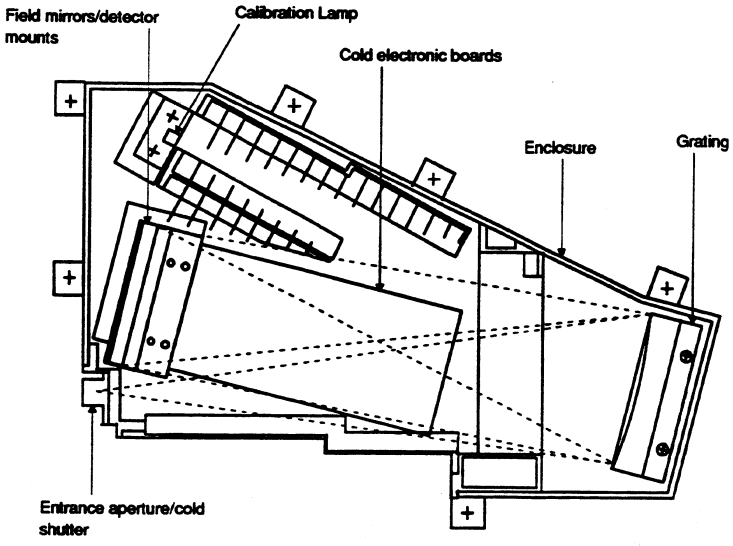

Figure 1. Schematic diagram of the optical layout of the *MIRS*

The *MIRS* had a cold shutter and a calibration source. In the survey observations the calibration sequence ran about once every 17.5 minutes, in which the shutter was closed and the calibration source was turned on. In the beginning of the observations, there were three periods during which the calibration sequences did not run due to operational commanding errors. The total observing time without calibration sequences was about

43 hours. The calibration source was intended to monitor the time variation in the sensitivity but was not employed for the in-flight absolute calibration. The contents of the calibration sequence are shown in Table 2. Unfortunately the shutter did not close completely and the fraction of the shutter closure was estimated from the background sky brightness (see section 4.2).

Table 1. *MIRS* calibration sequence[a]

Time (sec)[b]	Operation
0	Close the shutter
1	Reset
41	Turn on the calibration source
42	Reset
62	Turn off the calibration source
63	Open the shutter
64	Reset

a The calibration sequence ran every 17.5 minutes.
b The exact time unit is 1.024 sec.

There were several events that affected the quality of the *MIRS* data. The passage of the South Atlantic Anomaly (SAA) increased the noise significantly and a decrease in both the dark current and sensitivity was observed after the passage. These effects are described in Refs. 5 and 6 in detail. The data in the SAA passage are marked in the *MIRS* data file. The condensation of ^{3}He refrigerator of the Far-Infrared Photometer (FIRP) on board the *IRTS*[7] increased the focal plane temperature slightly, which affected the dark current of the *MIRS* detectors. There were two periods when the data recorder was saturated and thus the data were not taken. During these periods, the reset was not sent and thus right after the recorder recovery the detector output levels were not at a normal level. It took about 10 to 15 s for the outputs to recover to normal levels. The moon affected the *MIRS* data significantly. In particular, long-term after-effects were observed. Except for the SAA passages, no other flags are recorded in the *MIRS* data. These other events and periods are listed in Table 2.

We calibrated the *MIRS* prior to the launch in the laboratory as well as on orbit. The whole *IRTS* telescope was retrieved by the Space Shuttle about 10 months after launch and we also made calibration measurements of the *MIRS* instrument with the *IRTS* telescope after retrieval. The pre-launch and post-launch calibrations were consistent with each other. Table 3 summarizes which calibration was adopted for each instrument parameter of *MIRS*. Details of each calibration are described in subsequent sections.

3. INSTRUMENT PARAMETERS AND CALIBRATION

3.1. Wavelength calibration

Since there were no good objects for the *MIRS* wavelength calibration on orbit, we relied on the measurements in the laboratory for the wavelength calibration. The laboratory measurements were carried out by using the circular variable filters and interference filters.[3] The accuracy in the absolute wavelength is estimated to be better than 0.06 μm from the laboratory measurements. The detector channel and corresponding central wavelength are listed in Table 4.

3.2. Debias correction

Because of the nature of the integrated amplifier, the signal deviates from linearity as it fills up the capacity. This is called the debias effect. We made extensive measurements to characterize the debias effects in the laboratory. All the signals have been corrected for the debias effect based on the laboratory data. The correction was made according to the following formula.

$$\frac{dV_{cr}}{dt} = \frac{dV_{obs}}{dt} \times \{1 + (10 + V_{obs}) \times DB\}, \quad (1)$$

Table 2. Events affecting the *MIRS* data[a]

^{3}He condensation[b]		
03/30 10:25:29 – 03/31 00:45:39		
04/10 06:40:06 – 04/10 21:00:16		
After-effect of recorder saturation		
04/13 11:13:08 – 11:13:28		
04/16 23:46:10 – 23:46:56		
Periods during which the Moon may have affected the data		
04/08 13:12:03 – 13:17:01	04/10 02:49:09 – 02:58:36	04/21 20:24:54 – 20:33:40
04/08 14:47:09 – 14:51:01	04/10 04:24:29 – 04:32:33	04/21 21:59:27 – 22:08:43
04/08 16:20:37 – 16:25:25	04/10 05:58:25 – 06:06:32	04/21 23:33:55 – 23:42:03
04/08 17:54:46 – 17:59:40	04/10 07:33:01 – 07:40:50	04/22 01:07:47 – 01:16:21
04/08 19:28:20 – 19:34:00	04/10 09:07:24 – 09:14:36	04/22 02:42:17 – 02:50:28
04/08 21:01:58 – 21:08:33	04/10 10:41:34 – 10:48:34	04/22 04:16:37 – 04:30:44
04/08 22:36:13 – 22:42:56	04/10 12:16:07 – 12:22:33	04/22 05:50:47 – 06:08:24
04/09 00:11:41 – 00:17:32	04/10 13:51:10 – 13:56:23	04/22 07:25:07 – 07:33:14
04/09 03:18:22 – 03:25:41	04/10 15:25:39 – 15:30:24	04/22 08:57:06 – 09:07:38
04/09 06:25:48 – 06:34:14	04/10 17:01:10 – 17:04:00	04/22 12:07:24 – 12:14:40
04/09 08:00:26 – 08:08:29	04/10 18:34:49 – 18:37:55	04/22 13:42:09 – 13:49:42
04/09 09:34:38 – 09:42:46	04/10 20:09:17 – 20:11:21	04/22 15:16:29 – 15:25:04
04/09 11:08:51 – 12:08:42	04/21 01:37:48 – 01:40:19	04/22 16:51:37 – 16:58:34
04/09 12:43:02 – 12:56:06	04/21 03:11:38 – 03:15:54	04/22 18:25:03 – 18:32:16
04/09 14:17:44 – 14:25:28	04/21 04:45:26 – 04:50:50	04/22 19:58:59 – 20:06:59
04/09 15:51:23 – 15:59:14	04/21 06:18:54 – 06:24:47	04/22 21:33:13 – 21:41:53
04/09 17:25:41 – 17:35:36	04/21 07:52:41 – 07:59:05	04/22 23:08:16 – 23:15:06
04/09 18:59:24 – 19:07:43	04/21 12:36:16 – 12:42:04	04/22 23:07:59 – 23:15:05
04/09 20:33:55 – 20:42:44	04/21 14:08:44 – 14:17:10	04/23 00:43:32 – 00:48:06
04/09 22:08:14 – 22:16:05	04/21 15:42:57 – 15:51:02	04/23 02:17:17 – 02:22:15
04/09 23:42:19 – 23:50:03	04/21 17:17:00 – 17:25:29	
04/10 01:15:12 – 01:24:08	04/21 18:50:58 – 18:59:43	

a In the format of MM/DD hh:mm:ss in UT.
b Only in the later period of the condensation the *MIRS* detector temperature changed.

Table 3. *MIRS* parameter and the calibration method

Parameter	Calibration
Wavelength calibration	Laboratory measurement
Dark current	Flight data
Beam size	Laboratory measurement[a]
Debias correction	Laboratory measurement
Wavelength resolution	Calculation
Absolute flux calibration	Flight data

a The flight data confirmed the laboratory measurements.

where V_{obs} and V_{cr} are the observed and corrected signals, respectively, and DB is the debias correction factor. The signal ranges from -10 to $+10$ V. Table 5 lists the values of DBs. As can be seen, they are all of the order of a few $\times 10^{-3}\mathrm{V}^{-1}$. The V_{obs} was 5 V at most before resets (see section 2), thus the corrections were mostly a

Table 4. Detector channel and central wavelength

Channel number	Wavelength (μm)	Channel number	Wavelength (μm)	Channel number	Wavelength (μm)	Channel number	Wavelength (μm)
1	4.615	9	6.415	17	8.215	25	10.015
2	4.840	10	6.640	18	8.440	26	10.240
3	5.065	11	6.865	19	8.665	27	10.465
4	5.290	12	7.090	20	8.890	28	10.690
5	5.515	13	7.315	21	9.115	29	10.915
6	5.740	14	7.540	22	9.340	30	11.140
7	5.965	15	7.765	23	9.565	31	11.365
8	6.190	16	7.990	24	9.790	32	11.590

Table 5. Correction factor for the debias effect

Channel number	DB $\times 10^{-3}\mathrm{V}^{-1}$	Channel number	DB $\times 10^{-3}\mathrm{V}^{-1}$	Channel number	DB $\times 10^{-3}\mathrm{V}^{-1}$	Channel number	DB $\times 10^{-3}\mathrm{V}^{-1}$
1	4.54	9	4.66	17	4.35	25	4.46
2	4.45	10	5.18	18	4.60	26	4.47
3	4.28	11	4.76	19	4.83	27	4.37
4	4.21	12	4.98	20	4.52	28	4.21
5	4.20	13	5.53	21	4.52	29	4.44
6	5,26	14	4.92	22	4.70	30	4.31
7	4.12	15	4.44	23	3.44	31	4.16
8	4.39	16	4.85	24	4.03	32	4.52

few percent.

3.3. Beam size

The aperture of the *MIRS* was designed to be $8' \times 8'$ on the sky, which was confirmed in the laboratory measurements. In flight, the in-scan aperture size was measured by using point sources. It was found to be compatible with $8'$ with some wavelength dependence.[5] Estimation of the cross-scan size from the flight data was difficult because of the uncertainty in the pointing. Therefore we relied on the laboratory measurements for the aperture size. The total integrated signal was used in the in-flight absolute calibration (see section 3.5). Therefore, the in-scan aperture size does not affect the surface brightness directly. It is instead determined by the scan speed, which was well fixed by the satellite spin rate. Thus the major uncertainty in the absolute surface brightness comes from the cross-scan aperture size. We estimate the uncertainty in the aperture size measurements as better than 10%, including the uncertainty in the measurement setup.

3.4. Relative spectral response of each detector channel

The spectral resolution could not be determined by the in-flight data. The laboratory measurements did not provide very accurate data either since we did not have a sufficiently bright monochromatic light source. The computer simulation based on the measured parameters provided the most reliable and accurate relative spectral response for each detector channel and we adopted it for the wavelength resolution estimate.

Since the aperture size is large, the wavelength corresponding to a given detector channel depends on the source location in the entrance aperture as does the spectral response. Figure 2 shows an example of the dependence on the source location within the entrance aperture of channel #21. The calculation includes diffraction by the concave grating[4] and the transmission of the order-sorting filters. The latter gives only a very slow response change. Four thin lines indicate the relative spectral responses if a one-quarter rectangle

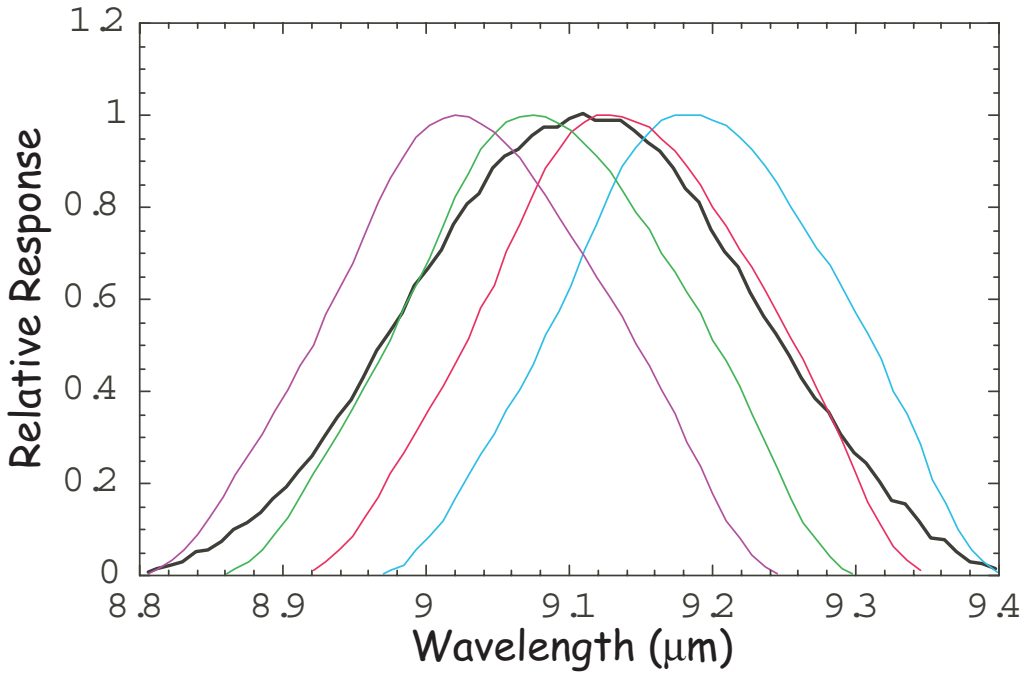

Figure 2. Relative spectral response of the #21 detector channel. The thick black line indicates the response for a diffuse source (the aperture is homogeneously illuminated), while the other four thin lines indicate the response when only one-quarter of the aperture is illuminated. For the *MIRS* calibration the black curve was adopted.

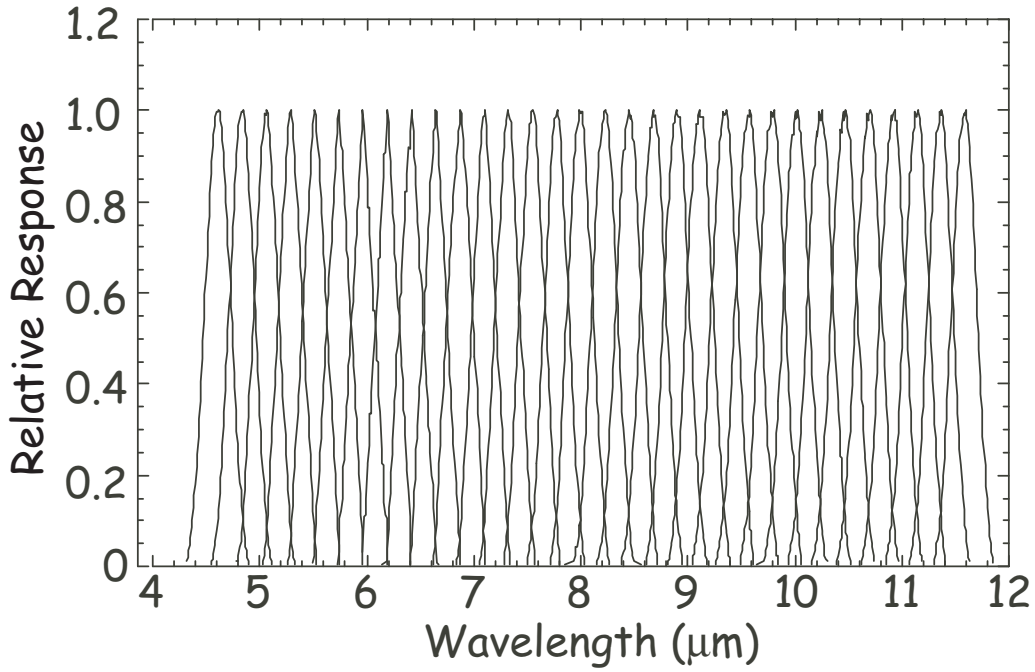

Figure 3. Relative spectral response of all the *MIRS* channels.

of the aperture ($2' \times 8'$) is illuminated homogeneously. The thick line indicates the response if the entire aperture is illuminated homogeneously, which is supposed to correspond to the relative spectral response for diffuse emission. Because of the uncertainty in the pointing we adopted the response for diffuse emission for point-sources as well. Figure 3 shows the relative spectral response of each detector for diffuse emission. The digital data are given in Table 6.

Table 6. Relative spectral response of *MIRS* channel

Channel 1		Channel 2		Channel 3		Channel 4		Channel 5		Channel 6		Channel 7		Channel 8	
μm	resp.	μm	resp.	μm	resp.	μm	resp.	μm	resp.	μm	resp.	μm	resp.	μm	resp.
4.3087	0.011	4.5429	0.002	4.7862	0.010	5.0204	0.002	5.2546	0.000	5.4979	0.009	5.7321	0.004	5.9664	0.033
4.3177	0.012	4.5519	0.012	4.7952	0.013	5.0294	0.012	5.2637	0.011	5.5069	0.024	5.7411	0.033	5.9754	0.111
4.3267	0.021	4.5609	0.016	4.8042	0.024	5.0384	0.023	5.2727	0.023	5.5159	0.047	5.7501	0.106	5.9844	0.112
4.3357	0.037	4.5700	0.027	4.8132	0.045	5.0474	0.038	5.2817	0.037	5.5249	0.095	5.7591	0.120	5.9934	0.150
4.3447	0.047	4.5790	0.047	4.8222	0.055	5.0564	0.058	5.2907	0.067	5.5339	0.132	5.7682	0.147	6.0024	0.224
4.3537	0.063	4.5880	0.056	4.8312	0.076	5.0655	0.083	5.2997	0.099	5.5429	0.162	5.7772	0.217	6.0114	0.225
4.3628	0.087	4.5970	0.079	4.8402	0.107	5.0745	0.115	5.3087	0.133	5.5519	0.211	5.7862	0.235	6.0204	0.265
4.3718	0.101	4.6060	0.107	4.8492	0.134	5.0835	0.151	5.3177	0.178	5.5609	0.249	5.7952	0.264	6.0294	0.336
4.3808	0.128	4.6150	0.124	4.8582	0.167	5.0925	0.185	5.3267	0.219	5.5700	0.281	5.8042	0.329	6.0384	0.337
4.3898	0.155	4.6240	0.159	4.8673	0.206	5.1015	0.229	5.3357	0.255	5.5790	0.325	5.8132	0.349	6.0474	0.381
4.3988	0.181	4.6330	0.196	4.8763	0.247	5.1105	0.273	5.3447	0.297	5.5880	0.365	5.8222	0.379	6.0564	0.449
4.4078	0.218	4.6420	0.220	4.8853	0.285	5.1195	0.306	5.3537	0.338	5.5970	0.397	5.8312	0.441	6.0655	0.450
4.4168	0.248	4.6510	0.264	4.8943	0.326	5.1285	0.353	5.3628	0.376	5.6060	0.442	5.8402	0.465	6.0745	0.498
4.4258	0.286	4.6600	0.308	4.9033	0.375	5.1375	0.399	5.3718	0.416	5.6150	0.481	5.8492	0.496	6.0835	0.563
4.4348	0.325	4.6691	0.341	4.9123	0.413	5.1465	0.429	5.3808	0.460	5.6240	0.514	5.8582	0.554	6.0925	0.563
4.4438	0.364	4.6781	0.386	4.9213	0.452	5.1555	0.476	5.3898	0.500	5.6330	0.561	5.8673	0.581	6.1015	0.615
4.4528	0.406	4.6871	0.440	4.9303	0.503	5.1646	0.523	5.3988	0.539	5.6420	0.597	5.8763	0.611	6.1105	0.676
4.4618	0.456	4.6961	0.471	4.9393	0.545	5.1736	0.552	5.4078	0.582	5.6510	0.633	5.8853	0.667	6.1195	0.677
4.4709	0.496	4.7051	0.518	4.9483	0.578	5.1826	0.599	5.4168	0.621	5.6600	0.679	5.8943	0.696	6.1285	0.733
4.4799	0.543	4.7141	0.573	4.9573	0.630	5.1916	0.648	5.4258	0.661	5.6691	0.715	5.9033	0.728	6.1375	0.790
4.4889	0.595	4.7231	0.605	4.9664	0.674	5.2006	0.677	5.4348	0.702	5.6781	0.755	5.9123	0.781	6.1465	0.792
4.4979	0.633	4.7321	0.651	4.9754	0.705	5.2096	0.723	5.4438	0.743	5.6871	0.798	5.9213	0.811	6.1555	0.855
4.5069	0.682	4.7411	0.706	4.9844	0.758	5.2186	0.771	5.4528	0.783	5.6961	0.831	5.9303	0.841	6.1646	0.904
4.5159	0.733	4.7501	0.745	4.9934	0.803	5.2276	0.804	5.4618	0.824	5.7051	0.874	5.9393	0.895	6.1736	0.909
4.5249	0.770	4.7591	0.784	5.0024	0.832	5.2366	0.848	5.4709	0.863	5.7141	0.915	5.9483	0.925	6.1826	0.976
4.5339	0.820	4.7682	0.840	5.0114	0.886	5.2456	0.897	5.4799	0.907	5.7231	0.950	5.9573	0.957	6.1916	1.000
4.5429	0.860	4.7772	0.877	5.0204	0.921	5.2546	0.929	5.4889	0.945	5.7321	0.982	5.9664	1.000	6.2006	0.975
4.5519	0.889	4.7862	0.906	5.0294	0.940	5.2637	0.964	5.4979	0.972	5.7411	1.000	5.9754	0.966	6.2096	0.930
4.5609	0.926	4.7952	0.944	5.0384	0.974	5.2727	0.987	5.5069	0.994	5.7501	0.980	5.9844	0.900	6.2186	0.888
4.5700	0.949	4.8042	0.967	5.0474	0.993	5.2817	0.995	5.5159	1.000	5.7591	0.925	5.9934	0.900	6.2276	0.862
4.5790	0.968	4.8132	0.983	5.0564	0.990	5.2907	1.000	5.5249	0.989	5.7682	0.912	6.0024	0.850	6.2366	0.805
4.5880	0.987	4.8222	0.999	5.0655	1.000	5.2997	0.989	5.5339	0.953	5.7772	0.874	6.0114	0.788	6.2456	0.777
4.5970	0.999	4.8312	0.996	5.0745	0.996	5.3087	0.970	5.5429	0.922	5.7862	0.810	6.0204	0.788	6.2546	0.750
4.6060	0.996	4.8402	0.998	5.0835	0.968	5.3177	0.939	5.5519	0.894	5.7952	0.794	6.0294	0.729	6.2637	0.688
4.6150	1.000	4.8492	1.000	5.0925	0.949	5.3267	0.902	5.5609	0.844	5.8042	0.757	6.0384	0.675	6.2727	0.663
4.6240	0.998	4.8582	0.978	5.1015	0.925	5.3357	0.866	5.5700	0.806	5.8132	0.695	6.0474	0.675	6.2817	0.636
4.6330	0.979	4.8673	0.957	5.1105	0.879	5.3447	0.824	5.5790	0.774	5.8222	0.676	6.0564	0.610	6.2907	0.571
4.6420	0.963	4.8763	0.938	5.1195	0.840	5.3537	0.782	5.5880	0.724	5.8312	0.635	6.0655	0.563	6.2997	0.551
4.6510	0.935	4.8853	0.896	5.1285	0.812	5.3628	0.742	5.5970	0.687	5.8402	0.580	6.0745	0.562	6.3087	0.522
4.6600	0.909	4.8943	0.861	5.1375	0.761	5.3718	0.699	5.6060	0.653	5.8492	0.557	6.0835	0.492	6.3177	0.457
4.6691	0.878	4.9033	0.827	5.1465	0.710	5.3808	0.658	5.6150	0.603	5.8582	0.517	6.0925	0.451	6.3267	0.440
4.6781	0.833	4.9123	0.782	5.1555	0.683	5.3898	0.619	5.6240	0.568	5.8673	0.465	6.1015	0.450	6.3357	0.408
4.6871	0.798	4.9213	0.735	5.1646	0.634	5.3988	0.576	5.6330	0.529	5.8763	0.440	6.1105	0.376	6.3447	0.343
4.6961	0.760	4.9303	0.698	5.1736	0.583	5.4078	0.534	5.6420	0.482	5.8853	0.398	6.1195	0.339	6.3537	0.327
4.7051	0.706	4.9393	0.650	5.1826	0.552	5.4168	0.495	5.6510	0.448	5.8943	0.349	6.1285	0.338	6.3628	0.288
4.7141	0.670	4.9483	0.601	5.1916	0.504	5.4258	0.452	5.6600	0.404	5.9033	0.322	6.1375	0.257	6.3718	0.225
4.7231	0.625	4.9573	0.562	5.2006	0.455	5.4348	0.409	5.6691	0.362	5.9123	0.281	6.1465	0.226	6.3808	0.212
4.7321	0.569	4.9664	0.518	5.2096	0.420	5.4438	0.371	5.6781	0.325	5.9213	0.230	6.1555	0.222	6.3898	0.166
4.7411	0.532	4.9754	0.466	5.2186	0.374	5.4528	0.328	5.6871	0.283	5.9303	0.202	6.1646	0.141	6.3988	0.111
4.7501	0.485	4.9844	0.429	5.2276	0.328	5.4618	0.284	5.6961	0.241	5.9393	0.160	6.1736	0.114	6.4078	0.100
4.7591	0.426	4.9934	0.383	5.2366	0.287	5.4709	0.247	5.7051	0.205	5.9483	0.112	6.1826	0.105	6.4168	0.047
4.7682	0.393	5.0024	0.331	5.2456	0.245	5.4799	0.204	5.7141	0.159	5.9573	0.084	6.1916	0.023		
4.7772	0.345	5.0114	0.295	5.2546	0.201	5.4889	0.160	5.7231	0.120	5.9664	0.042				
4.7862	0.296	5.0204	0.251	5.2637	0.168	5.4979	0.123	5.7321	0.084	5.9754	0.008				
4.7952	0.269	5.0294	0.210	5.2727	0.131	5.5069	0.088	5.7411	0.048						
4.8042	0.230	5.0384	0.179	5.2817	0.097	5.5159	0.062	5.7501	0.026						
4.8132	0.185	5.0474	0.144	5.2907	0.076	5.5249	0.036	5.7591	0.009						
4.8222	0.168	5.0564	0.115	5.2997	0.051	5.5339	0.020								
4.8312	0.134	5.0655	0.090	5.3087	0.031	5.5429	0.010								
4.8402	0.101	5.0745	0.065	5.3177	0.020										
4.8492	0.089	5.0835	0.047	5.3267	0.010										
4.8582	0.064	5.0925	0.035	5.3357	0.001										
4.8673	0.042	5.1015	0.020												
4.8763	0.037	5.1105	0.010												
4.8853	0.021	5.1195	0.006												
4.8943	0.011														
4.9033	0.009														

3.5. Absolute calibration for point sources

The absolute calibration of the *MIRS* was made based on in-flight observations of stars from M. Cohen's standard star network,[8] together with observations of Ceres. The standard stars used in the calibration of *MIRS* are listed in Table 7. We integrated the relative spectral response curves shown in Figure 3 over the absolute calibration spectra of stars and of Ceres to tie the MIRS to Cohen's standards. As described in the previous section, the wavelength for each observation depends on the cross-scan location in the aperture. This

Table 6. (continued)

Channel 9		Channel 10		Channel 11		Channel 12		Channel 13		Channel 14		Channel 15		Channel 16	
μm	resp.	μm	resp.	μm	resp.	μm	resp.	μm	resp.	μm	resp.	μm	resp.	μm	resp.
6.1826	0.013	6.3988	0.010	6.6150	0.009	6.8312	0.004	7.0474	0.002	7.2727	0.011	7.4889	0.008	7.7051	0.001
6.1916	0.041	6.4078	0.028	6.6240	0.023	6.8402	0.016	7.0564	0.012	7.2817	0.021	7.4979	0.012	7.7141	0.011
6.2006	0.081	6.4168	0.045	6.6330	0.042	6.8492	0.025	7.0655	0.022	7.2907	0.032	7.5069	0.019	7.7231	0.022
6.2096	0.130	6.4258	0.072	6.6420	0.063	6.8582	0.037	7.0745	0.033	7.2997	0.048	7.5159	0.035	7.7321	0.032
6.2186	0.159	6.4348	0.133	6.6510	0.093	6.8673	0.060	7.0835	0.055	7.3087	0.066	7.5249	0.049	7.7411	0.044
6.2276	0.208	6.4438	0.163	6.6600	0.136	6.8763	0.080	7.0925	0.079	7.3177	0.089	7.5339	0.058	7.7501	0.067
6.2366	0.247	6.4528	0.191	6.6691	0.184	6.8853	0.105	7.1015	0.099	7.3267	0.110	7.5429	0.084	7.7591	0.078
6.2456	0.278	6.4618	0.258	6.6781	0.225	6.8943	0.147	7.1105	0.133	7.3357	0.146	7.5519	0.109	7.7682	0.103
6.2546	0.339	6.4709	0.280	6.6871	0.267	6.9033	0.191	7.1195	0.173	7.3447	0.182	7.5609	0.123	7.7772	0.137
6.2637	0.364	6.4799	0.307	6.6961	0.320	6.9123	0.219	7.1285	0.211	7.3537	0.221	7.5700	0.158	7.7862	0.151
6.2727	0.398	6.4889	0.376	6.7051	0.356	6.9213	0.266	7.1375	0.265	7.3628	0.267	7.5790	0.196	7.7952	0.190
6.2817	0.465	6.4979	0.396	6.7141	0.396	6.9303	0.311	7.1465	0.304	7.3718	0.315	7.5880	0.226	7.8042	0.239
6.2907	0.482	6.5069	0.422	6.7231	0.447	6.9393	0.339	7.1555	0.344	7.3808	0.351	7.5970	0.271	7.8132	0.266
6.2997	0.520	6.5159	0.491	6.7321	0.479	6.9483	0.388	7.1646	0.395	7.3898	0.397	7.6060	0.318	7.8222	0.315
6.3087	0.590	6.5249	0.506	6.7411	0.521	6.9573	0.433	7.1736	0.434	7.3988	0.442	7.6150	0.350	7.8312	0.376
6.3177	0.600	6.5339	0.533	6.7501	0.566	6.9664	0.460	7.1826	0.474	7.4078	0.479	7.6240	0.397	7.8402	0.404
6.3267	0.641	6.5429	0.600	6.7591	0.596	6.9754	0.508	7.1916	0.523	7.4168	0.525	7.6330	0.443	7.8492	0.452
6.3357	0.712	6.5519	0.615	6.7682	0.638	6.9844	0.551	7.2006	0.561	7.4258	0.569	7.6420	0.481	7.8582	0.512
6.3447	0.719	6.5609	0.649	6.7772	0.675	6.9934	0.579	7.2096	0.602	7.4348	0.606	7.6510	0.529	7.8673	0.540
6.3537	0.760	6.5700	0.718	6.7862	0.705	7.0024	0.632	7.2186	0.646	7.4438	0.654	7.6600	0.575	7.8763	0.591
6.3628	0.824	6.5790	0.740	6.7952	0.748	7.0114	0.676	7.2276	0.685	7.4528	0.691	7.6691	0.615	7.8853	0.649
6.3718	0.824	6.5880	0.780	6.8042	0.779	7.0204	0.712	7.2366	0.723	7.4618	0.729	7.6781	0.664	7.8943	0.681
6.3808	0.862	6.5970	0.844	6.8132	0.811	7.0294	0.769	7.2456	0.766	7.4709	0.781	7.6871	0.712	7.9033	0.722
6.3898	0.921	6.6060	0.866	6.8222	0.851	7.0384	0.812	7.2546	0.807	7.4799	0.815	7.6961	0.752	7.9123	0.778
6.3988	0.918	6.6150	0.908	6.8312	0.875	7.0474	0.852	7.2637	0.847	7.4889	0.857	7.7051	0.801	7.9213	0.810
6.4078	0.954	6.6240	0.956	6.8402	0.899	7.0564	0.901	7.2727	0.886	7.4979	0.895	7.7141	0.843	7.9303	0.849
6.4168	1.000	6.6330	0.964	6.8492	0.931	7.0655	0.929	7.2817	0.920	7.5069	0.920	7.7231	0.879	7.9393	0.891
6.4258	0.988	6.6420	1.000	6.8582	0.955	7.0745	0.954	7.2907	0.952	7.5159	0.952	7.7321	0.917	7.9483	0.913
6.4348	0.954	6.6510	1.000	6.8673	0.970	7.0835	0.988	7.2997	0.972	7.5249	0.971	7.7411	0.942	7.9573	0.947
6.4438	0.899	6.6600	0.970	6.8763	1.000	7.0925	0.988	7.3087	0.980	7.5339	0.975	7.7501	0.967	7.9664	0.963
6.4528	0.877	6.6691	0.931	6.8853	0.993	7.1015	0.992	7.3177	1.000	7.5429	0.998	7.7591	0.981	7.9754	0.978
6.4618	0.840	6.6781	0.879	6.8943	0.970	7.1105	1.000	7.3267	0.999	7.5519	1.000	7.7682	0.988	7.9844	1.000
6.4709	0.776	6.6871	0.848	6.9033	0.936	7.1195	0.967	7.3357	0.983	7.5609	0.989	7.7772	1.000	7.9934	0.992
6.4799	0.756	6.6961	0.807	6.9123	0.898	7.1285	0.929	7.3447	0.976	7.5700	0.988	7.7862	0.989	8.0024	1.000
6.4889	0.719	6.7051	0.755	6.9213	0.871	7.1375	0.886	7.3537	0.941	7.5790	0.967	7.7952	0.977	8.0114	0.999
6.4979	0.657	6.7141	0.721	6.9303	0.832	7.1465	0.840	7.3628	0.894	7.5880	0.925	7.8042	0.971	8.0204	0.971
6.5069	0.638	6.7231	0.677	6.9393	0.792	7.1555	0.800	7.3718	0.852	7.5970	0.893	7.8132	0.930	8.0294	0.957
6.5159	0.599	6.7321	0.627	6.9483	0.764	7.1646	0.760	7.3808	0.808	7.6060	0.845	7.8222	0.888	8.0384	0.931
6.5249	0.535	6.7411	0.594	6.9573	0.716	7.1736	0.714	7.3898	0.761	7.6150	0.802	7.8312	0.853	8.0474	0.874
6.5339	0.516	6.7501	0.548	6.9664	0.674	7.1826	0.672	7.3988	0.719	7.6240	0.769	7.8402	0.797	8.0564	0.845
6.5429	0.477	6.7591	0.503	6.9754	0.638	7.1916	0.634	7.4078	0.678	7.6330	0.723	7.8492	0.755	8.0655	0.800
6.5519	0.416	6.7682	0.466	6.9844	0.587	7.2006	0.589	7.4168	0.631	7.6420	0.677	7.8582	0.719	8.0745	0.744
6.5609	0.403	6.7772	0.423	6.9934	0.547	7.2096	0.545	7.4258	0.586	7.6510	0.643	7.8673	0.665	8.0835	0.717
6.5700	0.363	6.7862	0.385	7.0024	0.512	7.2186	0.507	7.4348	0.551	7.6600	0.599	7.8763	0.622	8.0925	0.671
6.5790	0.309	6.7952	0.346	7.0114	0.460	7.2276	0.462	7.4438	0.505	7.6691	0.557	7.8853	0.583	8.1015	0.615
6.5880	0.294	6.8042	0.299	7.0204	0.425	7.2366	0.420	7.4528	0.459	7.6781	0.523	7.8943	0.532	8.1105	0.590
6.5970	0.249	6.8132	0.269	7.0294	0.390	7.2456	0.381	7.4618	0.428	7.6871	0.477	7.9033	0.489	8.1195	0.545
6.6060	0.199	6.8222	0.230	7.0384	0.335	7.2546	0.336	7.4709	0.378	7.6961	0.434	7.9123	0.446	8.1285	0.489
6.6150	0.181	6.8312	0.185	7.0474	0.299	7.2637	0.299	7.4799	0.337	7.7051	0.393	7.9213	0.398	8.1375	0.463
6.6240	0.128	6.8402	0.159	7.0564	0.260	7.2727	0.257	7.4889	0.305	7.7141	0.348	7.9303	0.352	8.1465	0.418
6.6330	0.084	6.8492	0.120	7.0655	0.197	7.2817	0.216	7.4979	0.256	7.7231	0.304	7.9393	0.313	8.1555	0.362
6.6420	0.064	6.8582	0.074	7.0745	0.160	7.2907	0.178	7.5069	0.216	7.7321	0.257	7.9483	0.267	8.1646	0.330
6.6510	0.009	6.8673	0.058	7.0835	0.124	7.2997	0.138	7.5159	0.183	7.7411	0.222	7.9573	0.223	8.1736	0.289
		6.8763	0.038	7.0925	0.078	7.3087	0.108	7.5249	0.145	7.7501	0.183	7.9664	0.194	8.1826	0.242
		6.8853	0.000	7.1015	0.056	7.3177	0.083	7.5339	0.115	7.7591	0.142	7.9754	0.161	8.1916	0.212
				7.1105	0.031	7.3267	0.054	7.5429	0.091	7.7682	0.116	7.9844	0.127	8.2006	0.178
						7.3357	0.033	7.5519	0.063	7.7772	0.088	7.9934	0.102	8.2096	0.143
						7.3447	0.013	7.5609	0.037	7.7862	0.053	8.0024	0.079	8.2186	0.118
								7.5700	0.023	7.7952	0.037	8.0114	0.056	8.2276	0.088
								7.5790	0.008	7.8042	0.020	8.0204	0.033	8.2366	0.066
												8.0294	0.022	8.2456	0.039
												8.0384	0.011	8.2546	0.025
														8.2637	0.013
														8.2727	0.000

effect is estimated to be 2–8% depending on the spectral shape of the object. Unfortunately the *IRTS* scan paths were not evenly spaced and the accuracy of the telescope pointing reconstruction was not sufficient ($\sim 2'$ rms in the cross-scan direction) to correct for this effect. In fact we found no systematic correlation of the flux with the cross-scan position in the aperture. Therefore for the present calibration we do not apply any corrections for the location of the source in the aperture and regard that effect as a random error. For the objects which have been observed more than once, the observations with low signals have been discarded and only the observations with high signals were used in the analysis. Those objects with multiple observations are thus expected to have better accuracy. The number of observations used is also listed in Table 7.

The flux of Ceres at the Earth varies with time. Fortunately enough, Ceres was observed from the Kuiper Airborne Observatory (April 14 and 19, 1995) within a few days of the *MIRS* observations (April 12 and 18, 1995). The *MIRS* observations of Ceres on April 12 were made right after passage through the SAA and may have been affected by the effects of the SAA (see section 4.1). These data show systematically low signals and have not been used in the calibration. The spectrum of Ceres is known to have fine structures at $\sim 10\,\mu$m[9] and these structures have been explicitly taken into account in the *MIRS* calibration through the real observed

Table 6. (continued)

Channel 17		Channel 18		Channel 19		Channel 20		Channel 21		Channel 22		Channel 23		Channel 24	
μm	resp.	μm	resp.	μm	resp.	μm	resp.	μm	resp.	μm	resp.	μm	resp.	μm	resp.
7.9303	0.011	8.1465	0.002	8.3718	0.010	8.5970	0.010	8.8042	0.001	9.0294	0.008	9.2546	0.011	9.4799	0.011
7.9393	0.012	8.1555	0.010	8.3808	0.010	8.6060	0.011	8.8132	0.012	9.0384	0.011	9.2637	0.011	9.4889	0.011
7.9483	0.022	8.1646	0.021	8.3898	0.020	8.6150	0.021	8.8222	0.018	9.0474	0.023	9.2727	0.021	9.4979	0.023
7.9573	0.044	8.1736	0.022	8.3988	0.030	8.6240	0.036	8.8312	0.025	9.0564	0.027	9.2817	0.031	9.5069	0.034
7.9664	0.045	8.1826	0.042	8.4078	0.041	8.6330	0.043	8.8402	0.048	9.0655	0.046	9.2907	0.043	9.5159	0.046
7.9754	0.067	8.1916	0.053	8.4168	0.055	8.6420	0.060	8.8492	0.053	9.0745	0.056	9.2997	0.053	9.5249	0.057
7.9844	0.089	8.2006	0.064	8.4258	0.071	8.6510	0.079	8.8582	0.070	9.0835	0.068	9.3087	0.072	9.5339	0.081
7.9934	0.102	8.2096	0.090	8.4348	0.088	8.6600	0.095	8.8673	0.097	9.0925	0.091	9.3177	0.087	9.5429	0.093
8.0024	0.134	8.2186	0.110	8.4438	0.109	8.6691	0.117	8.8763	0.113	9.1015	0.110	9.3267	0.106	9.5519	0.113
8.0114	0.158	8.2276	0.130	8.4528	0.130	8.6781	0.141	8.8853	0.132	9.1105	0.126	9.3357	0.130	9.5609	0.141
8.0204	0.184	8.2366	0.160	8.4618	0.159	8.6871	0.168	8.8943	0.163	9.1195	0.151	9.3447	0.145	9.5700	0.154
8.0294	0.228	8.2456	0.192	8.4709	0.189	8.6961	0.202	8.9033	0.190	9.1285	0.183	9.3537	0.179	9.5790	0.189
8.0384	0.261	8.2546	0.223	8.4799	0.215	8.7051	0.230	8.9123	0.224	9.1375	0.208	9.3628	0.208	9.5880	0.218
8.0474	0.293	8.2637	0.256	8.4889	0.252	8.7141	0.269	8.9213	0.257	9.1465	0.238	9.3718	0.231	9.5970	0.244
8.0564	0.348	8.2727	0.300	8.4979	0.294	8.7231	0.316	8.9303	0.296	9.1555	0.282	9.3808	0.278	9.6060	0.293
8.0655	0.391	8.2817	0.346	8.5069	0.332	8.7321	0.352	8.9393	0.341	9.1646	0.311	9.3898	0.309	9.6150	0.327
8.0745	0.427	8.2907	0.394	8.5159	0.375	8.7411	0.395	8.9483	0.377	9.1736	0.349	9.3988	0.344	9.6240	0.361
8.0835	0.484	8.2997	0.432	8.5249	0.423	8.7501	0.456	8.9573	0.427	9.1826	0.402	9.4078	0.403	9.6330	0.421
8.0925	0.524	8.3087	0.480	8.5339	0.464	8.7591	0.494	8.9664	0.486	9.1916	0.445	9.4168	0.442	9.6420	0.460
8.1015	0.562	8.3177	0.530	8.5429	0.505	8.7682	0.536	8.9754	0.523	9.2006	0.485	9.4258	0.483	9.6510	0.504
8.1105	0.620	8.3267	0.565	8.5519	0.551	8.7772	0.593	8.9844	0.568	9.2096	0.535	9.4348	0.542	9.6600	0.566
8.1195	0.661	8.3357	0.614	8.5609	0.597	8.7862	0.638	8.9934	0.625	9.2186	0.584	9.4438	0.585	9.6691	0.604
8.1285	0.697	8.3447	0.668	8.5700	0.642	8.7952	0.677	9.0024	0.665	9.2276	0.623	9.4528	0.624	9.6781	0.645
8.1375	0.754	8.3537	0.696	8.5790	0.688	8.8042	0.732	9.0114	0.703	9.2366	0.668	9.4618	0.680	9.6871	0.705
8.1465	0.795	8.3628	0.748	8.5880	0.735	8.8132	0.784	9.0204	0.761	9.2456	0.720	9.4709	0.729	9.6961	0.750
8.1555	0.821	8.3718	0.804	8.5970	0.779	8.8222	0.808	9.0294	0.803	9.2546	0.756	9.4799	0.763	9.7051	0.775
8.1646	0.879	8.3808	0.823	8.6060	0.816	8.8312	0.863	9.0384	0.825	9.2637	0.792	9.4889	0.812	9.7141	0.833
8.1736	0.909	8.3898	0.872	8.6150	0.852	8.8402	0.894	9.0474	0.881	9.2727	0.845	9.4979	0.854	9.7231	0.869
8.1826	0.922	8.3988	0.912	8.6240	0.893	8.8492	0.919	9.0564	0.906	9.2817	0.869	9.5069	0.877	9.7321	0.888
8.1916	0.959	8.4078	0.914	8.6330	0.902	8.8582	0.944	9.0655	0.922	9.2907	0.891	9.5159	0.900	9.7411	0.915
8.2006	0.971	8.4168	0.958	8.6420	0.939	8.8673	0.972	9.0745	0.953	9.2997	0.930	9.5249	0.940	9.7501	0.954
8.2096	0.984	8.4258	0.973	8.6510	0.963	8.8763	0.976	9.0835	0.972	9.3087	0.948	9.5339	0.950	9.7591	0.958
8.2186	0.996	8.4348	0.974	8.6600	0.964	8.8853	0.987	9.0925	0.971	9.3177	0.957	9.5429	0.960	9.7682	0.972
8.2276	1.000	8.4438	0.995	8.6691	0.982	8.8943	1.000	9.1015	0.988	9.3267	0.986	9.5519	0.991	9.7772	0.998
8.2366	1.000	8.4528	1.000	8.6781	1.000	8.9033	0.994	9.1105	1.000	9.3357	0.996	9.5609	0.992	9.7862	0.992
8.2456	0.992	8.4618	0.984	8.6871	0.985	8.9123	0.987	9.1195	0.987	9.3447	0.989	9.5700	0.985	9.7952	0.987
8.2546	0.973	8.4709	0.992	8.6961	0.989	8.9213	0.986	9.1285	0.987	9.3537	0.998	9.5790	1.000	9.8042	1.000
8.2637	0.954	8.4799	0.973	8.7051	0.987	8.9303	0.970	9.1375	0.984	9.3628	1.000	9.5880	0.990	9.8132	0.985
8.2727	0.920	8.4889	0.939	8.7141	0.951	8.9393	0.938	9.1465	0.961	9.3718	0.978	9.5970	0.970	9.8222	0.963
8.2817	0.885	8.4979	0.931	8.7231	0.940	8.9483	0.919	9.1555	0.936	9.3808	0.964	9.6060	0.959	9.8312	0.952
8.2907	0.843	8.5069	0.890	8.7321	0.908	8.9573	0.881	9.1646	0.919	9.3898	0.948	9.6150	0.939	9.8402	0.931
8.2997	0.783	8.5159	0.832	8.7411	0.850	8.9664	0.830	9.1736	0.883	9.3988	0.912	9.6240	0.898	9.8492	0.889
8.3087	0.748	8.5249	0.796	8.7501	0.816	8.9754	0.795	9.1826	0.839	9.4078	0.872	9.6330	0.864	9.8582	0.853
8.3177	0.709	8.5339	0.757	8.7591	0.776	8.9844	0.738	9.1916	0.807	9.4168	0.839	9.6420	0.827	9.8673	0.815
8.3267	0.645	8.5429	0.698	8.7682	0.715	8.9934	0.684	9.2006	0.747	9.4258	0.779	9.6510	0.765	9.8763	0.752
8.3357	0.611	8.5519	0.660	8.7772	0.674	9.0024	0.648	9.2096	0.699	9.4348	0.735	9.6600	0.722	9.8853	0.706
8.3447	0.573	8.5609	0.626	8.7862	0.640	9.0114	0.601	9.2186	0.666	9.4438	0.702	9.6691	0.684	9.8943	0.673
8.3537	0.511	8.5700	0.570	8.7952	0.578	9.0204	0.545	9.2276	0.611	9.4528	0.642	9.6781	0.625	9.9033	0.612
8.3628	0.475	8.5790	0.524	8.8042	0.529	9.0294	0.503	9.2366	0.561	9.4618	0.593	9.6871	0.579	9.9123	0.564
8.3718	0.438	8.5880	0.496	8.8132	0.503	9.0384	0.467	9.2456	0.523	9.4709	0.557	9.6961	0.538	9.9213	0.527
8.3808	0.378	8.5970	0.439	8.8222	0.441	9.0474	0.410	9.2546	0.476	9.4799	0.503	9.7051	0.485	9.9303	0.474
8.3898	0.340	8.6060	0.389	8.8312	0.388	9.0564	0.362	9.2637	0.425	9.4889	0.452	9.7141	0.436	9.9393	0.426
8.3988	0.304	8.6150	0.359	8.8402	0.366	9.0655	0.336	9.2727	0.383	9.4979	0.412	9.7231	0.394	9.9483	0.385
8.4078	0.254	8.6240	0.314	8.8492	0.314	9.0745	0.287	9.2817	0.354	9.5069	0.374	9.7321	0.356	9.9573	0.347
8.4168	0.225	8.6330	0.264	8.8582	0.264	9.0835	0.244	9.2907	0.303	9.5159	0.320	9.7411	0.307	9.9664	0.301
8.4258	0.192	8.6420	0.241	8.8673	0.245	9.0925	0.226	9.2997	0.264	9.5249	0.281	9.7501	0.265	9.9754	0.257
8.4348	0.152	8.6510	0.205	8.8763	0.207	9.1015	0.188	9.3087	0.242	9.5339	0.256	9.7591	0.245	9.9844	0.242
8.4438	0.130	8.6600	0.159	8.8853	0.157	9.1105	0.144	9.3177	0.202	9.5429	0.213	9.7682	0.201	9.9934	0.195
8.4528	0.100	8.6691	0.141	8.8943	0.146	9.1195	0.138	9.3267	0.158	9.5519	0.170	9.7772	0.163	10.0024	0.159
8.4618	0.075	8.6781	0.108	8.9033	0.112	9.1285	0.104	9.3357	0.152	9.5609	0.160	9.7862	0.152	10.0114	0.149
8.4709	0.052	8.6871	0.079	8.9123	0.076	9.1375	0.069	9.3447	0.114	9.5700	0.120	9.7952	0.114	10.0204	0.112
8.4799	0.033	8.6961	0.061	8.9213	0.063	9.1465	0.064	9.3537	0.077	9.5790	0.083	9.8042	0.080	10.0294	0.079
8.4889	0.023	8.7051	0.040	8.9303	0.042	9.1555	0.044	9.3628	0.073	9.5880	0.078	9.8132	0.073	10.0384	0.072
8.4979	0.011	8.7141	0.026	8.9393	0.025	9.1646	0.022	9.3718	0.050	9.5970	0.052	9.8222	0.049	10.0474	0.049
		8.7231	0.013	8.9483	0.014	9.1736	0.015	9.3808	0.025	9.6060	0.027	9.8312	0.025	10.0564	0.025
				8.9573	0.001	9.1826	0.004	9.3898	0.021	9.6150	0.023	9.8402	0.022	10.0655	0.021
								9.3988	0.011	9.6240	0.013	9.8492	0.012	10.0745	0.012

data. The absolute flux level of the KAO Ceres data is in good agreement with the Standard Thermal Model prediction (K.-W. Chan, private communication).[10]

The signals for point sources were obtained from the difference in the voltage level between before and after the source was observed, after corrections for dark current during the time of the transit of the object across the aperture. We have obtained the conversion factor for point sources, C_p, from the observed integrated signal in Volts into the flux density unit Jansky (Jy) for each channel by a least-squares fit. The data and fit curves are plotted in Figure 4 and the conversion factors and their errors used for the catalog production are listed in Table 8. As can been seen, the calibration for shorter wavelength channels is primarily based on several bright standard stars, while that for longer wavelength channels relies mostly on only one bright object, Ceres. The good agreement seen in the in-between spectral channels confirms that this process does not introduce serious systematic errors in longer wavelength channels, but the weakness of the *MIRS* calibration in the longer wavelength channels should not be overlooked. The fits in Figure 4 and Table 8 indicate the internal consistency

Table 6. (continued)

Channel 25		Channel 26		Channel 27		Channel 28		Channel 29		Channel 30		Channel 31		Channel 32	
μm	resp.	μm	resp.	μm	resp.	μm	resp.	μm	resp.	μm	resp.	μm	resp.	μm	resp.
9.7051	0.012	9.9303	0.012	10.1555	0.012	10.3808	0.005	10.6060	0.000	10.8402	0.011	11.0655	0.010	11.2997	0.013
9.7141	0.012	9.9393	0.012	10.1646	0.012	10.3898	0.012	10.6150	0.011	10.8492	0.011	11.0745	0.012	11.3087	0.018
9.7231	0.023	9.9483	0.024	10.1736	0.024	10.3988	0.022	10.6240	0.013	10.8582	0.023	11.0835	0.024	11.3177	0.026
9.7321	0.035	9.9573	0.036	10.1826	0.035	10.4078	0.026	10.6330	0.022	10.8673	0.034	11.0925	0.031	11.3267	0.052
9.7411	0.047	9.9664	0.048	10.1916	0.048	10.4168	0.044	10.6420	0.034	10.8763	0.045	11.1015	0.049	11.3357	0.058
9.7501	0.059	9.9754	0.060	10.2006	0.060	10.4258	0.056	10.6510	0.045	10.8853	0.057	11.1105	0.061	11.3447	0.079
9.7591	0.083	9.9844	0.085	10.2096	0.081	10.4348	0.065	10.6600	0.056	10.8943	0.080	11.1195	0.078	11.3537	0.104
9.7682	0.096	9.9934	0.097	10.2186	0.097	10.4438	0.091	10.6691	0.079	10.9033	0.092	11.1285	0.099	11.3628	0.121
9.7772	0.112	10.0024	0.111	10.2276	0.109	10.4528	0.101	10.6781	0.091	10.9123	0.116	11.1375	0.125	11.3718	0.144
9.7862	0.144	10.0114	0.147	10.2366	0.137	10.4618	0.121	10.6871	0.114	10.9213	0.140	11.1465	0.140	11.3808	0.183
9.7952	0.157	10.0204	0.160	10.2456	0.158	10.4709	0.150	10.6961	0.137	10.9303	0.166	11.1555	0.177	11.3898	0.201
9.8042	0.188	10.0294	0.189	10.2546	0.186	10.4799	0.175	10.7051	0.162	10.9393	0.191	11.1646	0.203	11.3988	0.237
9.8132	0.221	10.0384	0.222	10.2637	0.213	10.4889	0.198	10.7141	0.187	10.9483	0.227	11.1736	0.232	11.4078	0.290
9.8222	0.247	10.0474	0.251	10.2727	0.249	10.4979	0.237	10.7231	0.224	10.9573	0.266	11.1826	0.282	11.4168	0.321
9.8312	0.294	10.0564	0.294	10.2817	0.285	10.5069	0.274	10.7321	0.261	10.9664	0.294	11.1916	0.322	11.4258	0.367
9.8402	0.324	10.0655	0.323	10.2907	0.315	10.5159	0.298	10.7411	0.286	10.9754	0.341	11.2006	0.352	11.4348	0.423
9.8492	0.363	10.0745	0.367	10.2997	0.366	10.5249	0.350	10.7501	0.335	10.9844	0.391	11.2096	0.413	11.4438	0.471
9.8582	0.423	10.0835	0.425	10.3087	0.418	10.5339	0.399	10.7591	0.385	10.9934	0.444	11.2186	0.468	11.4528	0.508
9.8673	0.453	10.0925	0.454	10.3177	0.451	10.5429	0.433	10.7682	0.424	11.0024	0.478	11.2276	0.493	11.4618	0.568
9.8763	0.504	10.1015	0.509	10.3267	0.508	10.5519	0.488	10.7772	0.473	11.0114	0.529	11.2366	0.553	11.4709	0.609
9.8853	0.564	10.1105	0.569	10.3357	0.562	10.5609	0.537	10.7862	0.523	11.0204	0.592	11.2456	0.616	11.4799	0.644
9.8943	0.602	10.1195	0.598	10.3447	0.595	10.5700	0.580	10.7952	0.570	11.0294	0.619	11.2546	0.635	11.4889	0.705
9.9033	0.643	10.1285	0.649	10.3537	0.648	10.5790	0.626	10.8042	0.610	11.0384	0.668	11.2637	0.691	11.4979	0.743
9.9123	0.704	10.1375	0.708	10.3628	0.700	10.5880	0.674	10.8132	0.661	11.0474	0.732	11.2727	0.753	11.5069	0.778
9.9213	0.748	10.1465	0.748	10.3718	0.746	10.5970	0.725	10.8222	0.715	11.0564	0.757	11.2817	0.778	11.5159	0.838
9.9303	0.771	10.1555	0.776	10.3808	0.778	10.6060	0.761	10.8312	0.751	11.0655	0.796	11.2907	0.823	11.5249	0.866
9.9393	0.832	10.1646	0.836	10.3898	0.829	10.6150	0.802	10.8402	0.790	11.0745	0.860	11.2997	0.876	11.5339	0.890
9.9483	0.864	10.1736	0.871	10.3988	0.877	10.6240	0.850	10.8492	0.843	11.0835	0.871	11.3087	0.888	11.5429	0.936
9.9573	0.879	10.1826	0.883	10.4078	0.887	10.6330	0.869	10.8582	0.857	11.0925	0.901	11.3177	0.926	11.5519	0.951
9.9664	0.912	10.1916	0.920	10.4168	0.918	10.6420	0.901	10.8673	0.893	11.1015	0.941	11.3267	0.950	11.5609	0.971
9.9754	0.949	10.2006	0.955	10.4258	0.959	10.6510	0.942	10.8763	0.927	11.1105	0.950	11.3357	0.961	11.5700	0.982
9.9844	0.947	10.2096	0.944	10.4348	0.949	10.6600	0.939	10.8853	0.939	11.1195	0.963	11.3447	0.976	11.5790	0.994
9.9934	0.971	10.2186	0.975	10.4438	0.972	10.6691	0.962	10.8943	0.952	11.1285	0.997	11.3537	0.996	11.5880	0.990
10.0024	0.998	10.2276	0.997	10.4528	1.000	10.6781	0.993	10.9033	0.991	11.1375	0.986	11.3628	0.989	11.5970	1.000
10.0114	0.984	10.2366	0.979	10.4618	0.978	10.6871	0.979	10.9123	0.980	11.1465	1.000	11.3718	1.000	11.6060	0.983
10.0204	0.987	10.2456	0.988	10.4709	0.990	10.6961	0.992	10.9213	0.993	11.1555	0.999	11.3808	0.986	11.6150	0.971
10.0294	1.000	10.2546	1.000	10.4799	1.000	10.7051	1.000	10.9303	1.000	11.1646	0.982	11.3898	0.969	11.6240	0.961
10.0384	0.980	10.2637	0.980	10.4889	0.984	10.7141	0.990	10.9393	0.979	11.1736	0.973	11.3988	0.951	11.6330	0.919
10.0474	0.961	10.2727	0.961	10.4979	0.963	10.7231	0.976	10.9483	0.977	11.1826	0.945	11.4078	0.924	11.6420	0.890
10.0564	0.951	10.2817	0.950	10.5069	0.947	10.7321	0.953	10.9573	0.956	11.1916	0.905	11.4168	0.882	11.6510	0.849
10.0655	0.931	10.2907	0.932	10.5159	0.934	10.7411	0.928	10.9664	0.916	11.2006	0.882	11.4258	0.852	11.6600	0.795
10.0745	0.887	10.2997	0.888	10.5249	0.891	10.7501	0.904	10.9754	0.903	11.2096	0.835	11.4348	0.802	11.6691	0.747
10.0835	0.844	10.3087	0.842	10.5339	0.848	10.7591	0.857	10.9844	0.855	11.2186	0.775	11.4438	0.748	11.6781	0.693
10.0925	0.813	10.3177	0.809	10.5429	0.807	10.7682	0.800	10.9934	0.789	11.2276	0.732	11.4528	0.706	11.6871	0.651
10.1015	0.751	10.3267	0.751	10.5519	0.757	10.7772	0.772	11.0024	0.763	11.2366	0.688	11.4618	0.659	11.6961	0.608
10.1105	0.700	10.3357	0.699	10.5609	0.707	10.7862	0.718	11.0114	0.717	11.2456	0.634	11.4709	0.608	11.7051	0.550
10.1195	0.669	10.3447	0.665	10.5700	0.656	10.7952	0.658	11.0204	0.651	11.2546	0.586	11.4799	0.561	11.7141	0.512
10.1285	0.611	10.3537	0.610	10.5790	0.617	10.8042	0.632	11.0294	0.619	11.2637	0.547	11.4889	0.509	11.7231	0.474
10.1375	0.561	10.3628	0.561	10.5880	0.568	10.8132	0.581	11.0384	0.576	11.2727	0.495	11.4979	0.471	11.7321	0.416
10.1465	0.523	10.3718	0.514	10.5970	0.510	10.8222	0.514	11.0474	0.513	11.2817	0.441	11.5069	0.423	11.7411	0.379
10.1555	0.473	10.3808	0.473	10.6060	0.479	10.8312	0.493	11.0564	0.477	11.2907	0.408	11.5159	0.376	11.7501	0.343
10.1646	0.421	10.3898	0.420	10.6150	0.427	10.8402	0.439	11.0655	0.432	11.2997	0.359	11.5249	0.336	11.7591	0.285
10.1736	0.378	10.3988	0.363	10.6240	0.366	10.8492	0.372	11.0745	0.373	11.3087	0.312	11.5339	0.289	11.7682	0.255
10.1826	0.346	10.4078	0.345	10.6330	0.351	10.8582	0.357	11.0835	0.340	11.3177	0.279	11.5429	0.257	11.7772	0.224
10.1916	0.299	10.4168	0.295	10.6420	0.301	10.8673	0.307	11.0925	0.297	11.3267	0.243	11.5519	0.222	11.7862	0.176
10.2006	0.251	10.4258	0.242	10.6510	0.246	10.8763	0.252	11.1015	0.256	11.3357	0.198	11.5609	0.175	11.7952	0.148
10.2096	0.240	10.4348	0.237	10.6600	0.239	10.8853	0.233	11.1105	0.223	11.3447	0.167	11.5700	0.161	11.8042	0.129
10.2186	0.192	10.4438	0.190	10.6691	0.195	10.8943	0.193	11.1195	0.189	11.3537	0.144	11.5790	0.126	11.8132	0.091
10.2276	0.157	10.4528	0.149	10.6781	0.153	10.9033	0.157	11.1285	0.155	11.3628	0.110	11.5880	0.090	11.8222	0.068
10.2366	0.148	10.4618	0.146	10.6871	0.140	10.9123	0.131	11.1375	0.128	11.3718	0.084	11.5970	0.077	11.8312	0.053
10.2456	0.111	10.4709	0.110	10.6961	0.108	10.9213	0.105	11.1465	0.101	11.3808	0.063	11.6060	0.055	11.8402	0.032
10.2546	0.077	10.4799	0.073	10.7051	0.075	10.9303	0.077	11.1555	0.075	11.3898	0.043	11.6150	0.033	11.8492	0.021
10.2637	0.071	10.4889	0.065	10.7141	0.052	10.9393	0.052	11.1646	0.050	11.3988	0.023	11.6240	0.022	11.8582	0.009
10.2727	0.048	10.4979	0.047	10.7231	0.042	10.9483	0.039	11.1736	0.028	11.4078	0.011	11.6330	0.011		
10.2817	0.024	10.5069	0.024	10.7321	0.025	10.9573	0.026	11.1826	0.023	11.4168	0.000				
10.2907	0.017	10.5159	0.013	10.7411	0.012	10.9664	0.013	11.1916	0.012						
10.2997	0.011	10.5249	0.005												

of the current absolute flux calibration to be about 5–10%.

3.6. Absolute calibration for diffuse sources

The absolute calibration for the diffuse emission was made based on the point source calibration. The conversion factor for the diffuse sources, C_d, is derived in units of MJy sr^{-1} (V s^{-1})$^{-1}$. We assume that the cross-scan direction beam size is 8′ and that the spin rate of the satellite is 3.′824 s^{-1}. Then C_d can be calculated as

$$C_d[\mathrm{MJy\ sr^{-1}}] = C_p[\mathrm{Jy\ V^{-1}}] \times 10^{-6}/(3'.824 \times 8')/(\pi/180.0/60.0)^2. \quad (2)$$

The values of C_d together with the errors are also listed in Table 8.

Table 7. List of the standard stars used for the *MIRS* calibration

Object	# of Obs.[a]	Object	# of Obs.[a]	Object	#r of Obs.[a]	Object	# of Obs.[a]
HD8810	5	HD25422	2	HD27442	2	HD29317	2
HD30185	5	HD33042	2	HD33116	1	HD40091	2
HD40808	2	HD42682	1	HD43785	1	HD44951	2
HD46431	2	HD46815	2	HD47205	5	HD47536	2
HD59381	3	HD66141	15	HD72094	5	HD72292	3
HD75716	5	HD91496	2	HD137066	1	HD137759	1
HD138538	2	HD142676	4	HD157325	2	HD163770	10
HD163917	6	HD164646	6	HD168775	1	HD173780	7
HD176527	6	HD184406	2	HD192781	3	HD198542	3
HD217902	9	HD220263	1	Ceres	4		

a The number of observations used for the calibration.

4. ANOMALIES

4.1. Effect of the South Atlantic Anomaly

The responsivity of the *MIRS* detectors were severely affected by passages through the SAA, where a large increase in the ionizing radiation hits was observed.[5] Figure 5 shows the hit count map estimated from the *MIRS* data (see section 5). The detector responsivity was monitored by the *MIRS* internal calibration source and found to decrease for a period of time following passages of the SAA. Typical behavior of the *MIRS* detectors after the SAA passage is shown in Figure 6. The changes are well-fit by an equation of $R(t) = R_0[1 - A\exp(-t/\tau)]$, where R_0 is the normal detector responsivity, A is a constant describing the magnitude of the change just after exiting the SAA, τ is a time-constant of the change, and t is the time after exiting the SAA. Typical values of A are $0.7 - 0.8$ and the time constant τ ranges $1000 - 1500$ s, depending on the detector. Thus after 500 s from the exit of the SAA, the change becomes less than 10%. In the present data reduction the data taken within 500 s after the exit of the SAA are discarded.

4.2. Dark current

In the calibration sequence, the shutter was not closed completely. Therefore, the signal during the shutter close consists of the dark current and the signal from the sky background. The measured signal during the shutter open should be written by

$$S_{\rm open} = S_{\rm dark} + R \times B_{\rm sky}, \tag{3}$$

where $S_{\rm dark}$ indicates the dark current, R is the responsivity, and $B_{\rm sky}$ is the sky brightness. The signal during the shutter close is given by

$$S_{\rm close} = S_{\rm dark} + R \times B_{\rm sky} \times (1 - f), \tag{4}$$

where f is the fraction with which the shutter is closed. In practice $S_{\rm dark}$ also includes the effects of thermal radiation from anything warm inside the *MIRS* enclosure. Then from Eqs. (3) and (4) we obtain,

$$S_{\rm close} = f \times S_{\rm dark} + (1 - f) \times S_{\rm open}. \tag{5}$$

Thus the slope of the plot of $S_{\rm open}$ versus $S_{\rm close}$ gives $1 - f$ if we assume that f does not change during the flight and that the variation in $S_{\rm dark}$ is much smaller than that in $B_{\rm sky}$, which holds true for the *MIRS* observations. From the fit we obtained $f \sim 0.55 \pm 0.03$. This value is currently used for the data reduction of the diffuse emission.

Table 8. Conversion Factor

Channel Number	Center Wavelength (μm)	Conversion Factor for point source C_p (Jy V^{-1})	Uncertainty in C_p (Jy V^{-1})	Conversion Factor for diffuse source C_d (MJy (V s^{-1})$^{-1}$)	Uncertainty in C_d (MJy (V s^{-1})$^{-1}$)
1	4.615	2.806E+03	4.162E+01	1.084E+03	1.608E+01
2	4.840	3.295E+03	4.769E+01	1.273E+03	1.842E+01
3	5.065	3.978E+03	8.022E+01	1.537E+03	3.099E+01
4	5.290	2.419E+03	3.029E+01	9.345E+02	1.170E+01
5	5.515	4.225E+03	8.499E+01	1.632E+03	3.283E+01
6	5.740	3.278E+03	5.869E+01	1.266E+03	2.267E+01
7	5.965	1.984E+03	3.067E+01	7.664E+02	1.185E+01
8	6.190	1.839E+03	2.538E+01	7.104E+02	9.805E+00
9	6.415	2.461E+03	3.762E+01	9.507E+02	1.453E+01
10	6.640	3.852E+03	7.148E+01	1.488E+03	2.761E+01
11	6.865	2.318E+03	3.917E+01	8.955E+02	1.513E+01
12	7.090	1.943E+03	2.917E+01	7.506E+02	1.127E+01
13	7.315	2.493E+03	4.452E+01	9.631E+02	1.720E+01
14	7.540	2.402E+03	3.212E+01	9.279E+02	1.241E+01
15	7.765	2.746E+03	4.079E+01	1.061E+03	1.576E+01
16	7.990	2.362E+03	2.805E+01	9.125E+02	1.084E+01
17	8.215	2.693E+03	3.825E+01	1.040E+03	1.478E+01
18	8.440	3.143E+03	4.199E+01	1.214E+03	1.622E+01
19	8.665	4.279E+03	6.209E+01	1.653E+03	2.399E+01
20	8.890	4.968E+03	6.829E+01	1.919E+03	2.638E+01
21	9.115	6.688E+03	1.077E+02	2.584E+03	4.161E+01
22	9.340	5.207E+03	6.977E+01	2.012E+03	2.695E+01
23	9.565	6.438E+03	9.955E+01	2.487E+03	3.846E+01
24	9.790	5.942E+03	7.334E+01	2.295E+03	2.833E+01
25	10.015	7.595E+03	9.294E+01	2.934E+03	3.590E+01
26	10.240	9.227E+03	2.078E+02	3.565E+03	8.028E+01
27	10.465	1.004E+04	1.658E+02	3.879E+03	6.405E+01
28	10.690	1.353E+04	1.167E+02	5.227E+03	4.508E+01
29	10.915	9.195E+03	1.402E+02	3.552E+03	5.416E+01
30	11.140	1.118E+04	2.114E+02	4.319E+03	8.167E+01
31	11.365	1.435E+04	5.092E+02	5.544E+03	1.967E+02
32	11.590	1.252E+04	3.588E+02	4.837E+03	1.386E+02

The dark current was found to change also after passages of the SAA. The change of the dark current is presently only approximately taken into account in the data reduction and will be further refined in the next *MIRS* calibration release. The uncertainty in the dark current estimate affects the absolute flux of the surface brightness. Table 9 lists the current estimate of the uncertainty due to the dark current.

4.3. Other anomalies

The signals showed anomalies immediately following a reset and the data within 2.048 s after the reset were not used in the present data reduction. We noticed that the dark current and responsivity was slightly higher in the beginning phase of the observations, originating from a change in detector temperature compared with later in the mission. We also noticed that ^{3}He condensation of the FIRP refrigerator and passages of the moon changed the temperature of the *MIRS* and thus affected the dark current and responsivity. However these effects are relatively small (less than 5%) and are not included in the current calibration.

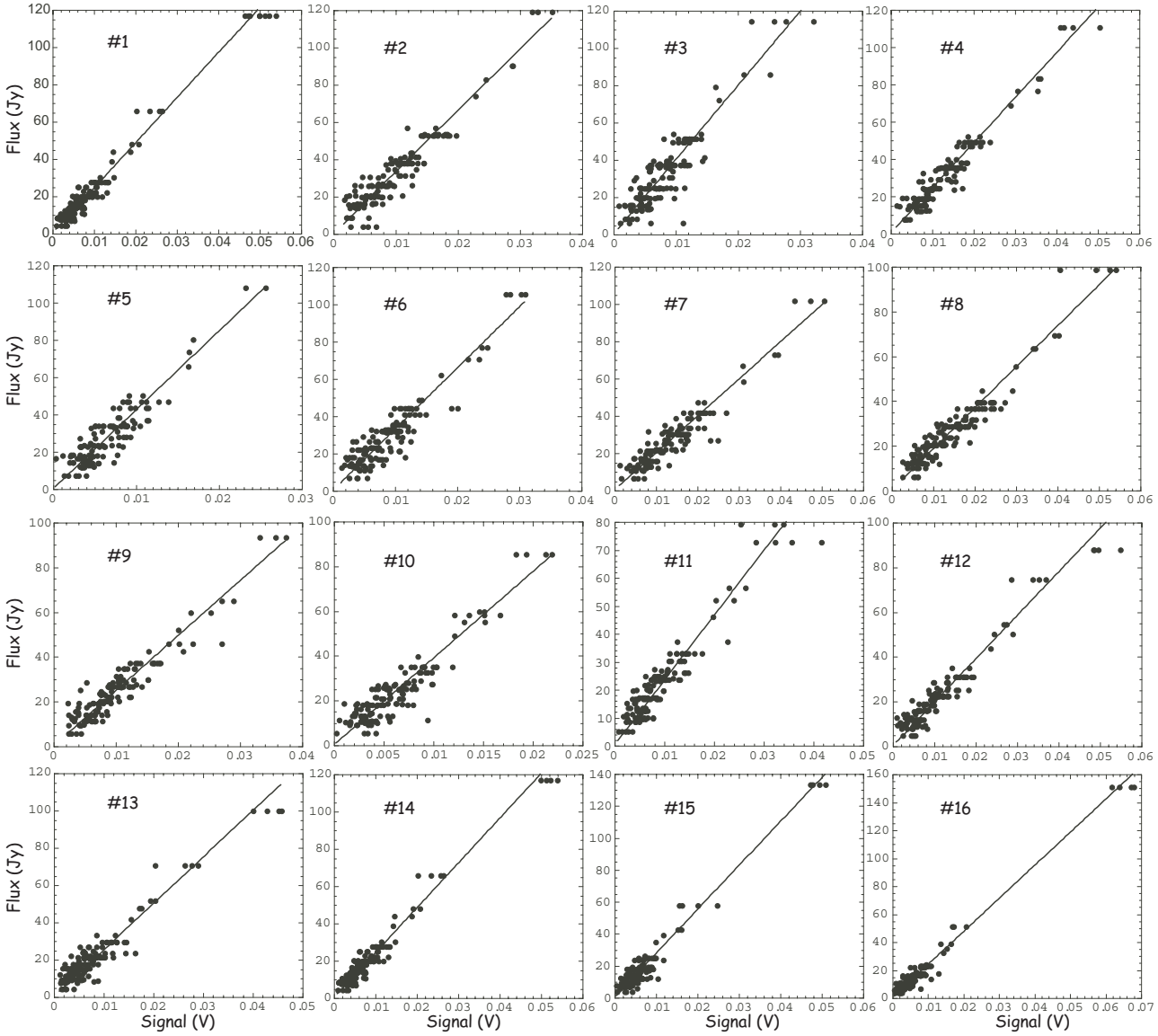

Figure 4. Flux to signal plots for the standard star observations

5. POINT SOURCE EXTRACTION

The point source extraction of the *MIRS* data was carried out in three steps: creating an event list, deriving the flux of each event, and averaging the fluxes of the same object. Each procedure is described in the following.

The original *MIRS* data were the integrated signals. This dataset is called the BDM (Binary Dumped MIRS) data. During the creation of the BDM dataset, the cosmic ray hits were examined and corrected (despiking). The hit rate of high-energy particles was also calculated, from which the location of the SAA was estimated and the hit rate map was created. In most cases it is easier to look at the differentiated signals rather than the integrated signals. The DIF (Differentiated) dataset were prepared by 5-point weighted differentiation of the BDM data for this purpose.

The event detections of the *MIRS* data were made from the DIF dataset. The data during the calibration sequences and SAA passages were not used in the event detection process. The data with the moon avoidance

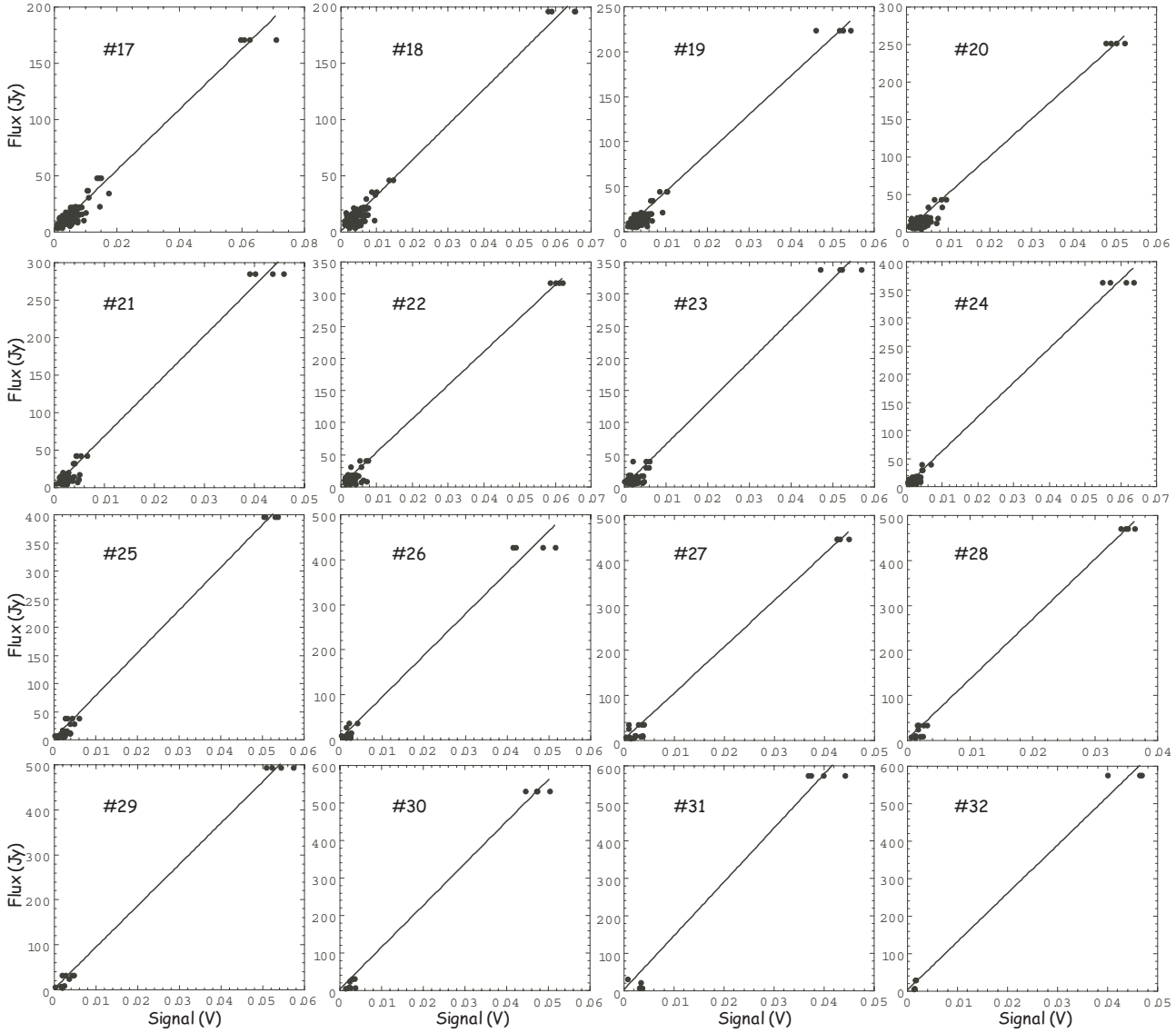

Figure 4. (continued)

angle less than 10 degrees were also not processed because of the possible contamination by strong light from the moon. The event detection was made basically with a Zero-Sum Square-Wave Filter (ZSSWF).[11] In addition, bright signals relative to the background noise were also registered. These signals were further examined and spurious signals due to the high-energy particle hits, which had not been corrected in despiking the BDM dataset, were rejected. The rejection was made primarily based on the width of the event in the time frame as well as in the spectral frame since cosmic ray hits generally affected only one detector for one read, unlike a real source. The final selection parameters were adjusted with the local noise level and also the sampling rate (see section 2). This process finally provided the event list, which included the start, end, and weighted center of the event together with the rough estimate of the integrated signal. We had 10451 events detected by the present algorithm.

The calculation of the flux for each event was made with the BDM dataset. The background signal level was estimated by the fitting of linear lines before and after the event and the difference in the offset was registered

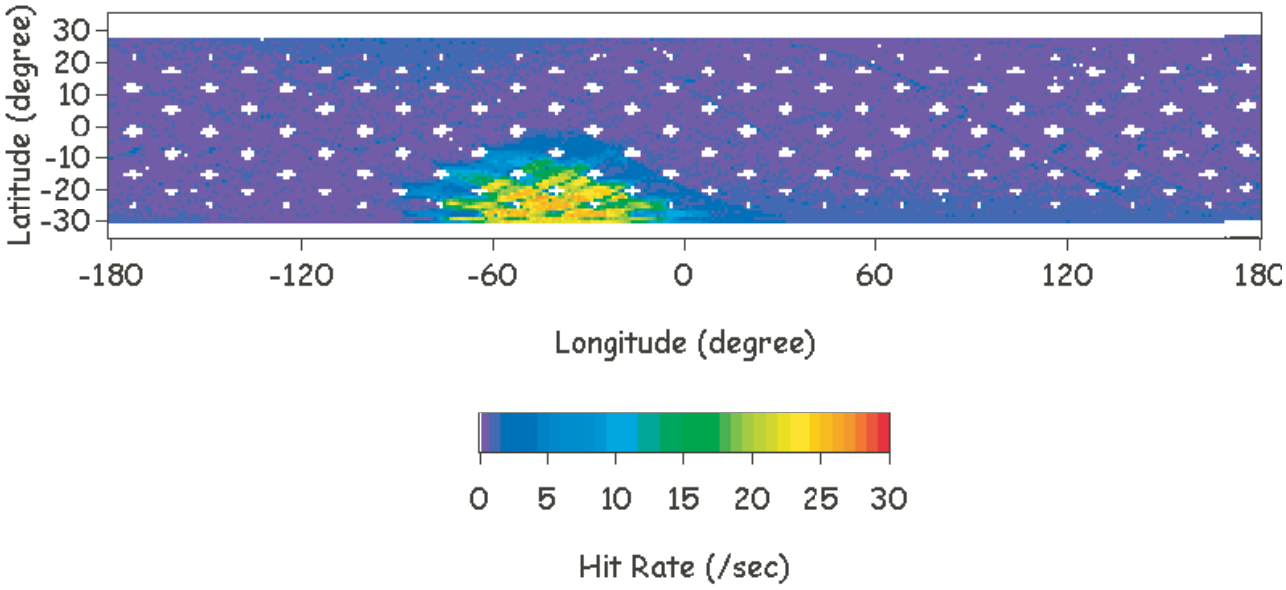

Figure 5. Energetic particle hit rate for the *MIRS* detectors. The white spots indicate those regions where the *IRTS* orbit did not pass that portion of the earth's surface.

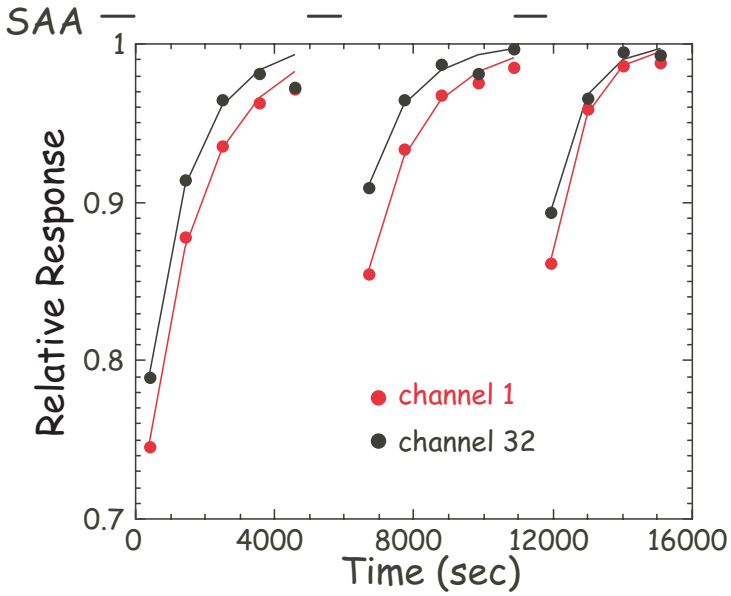

Figure 6. Variation in the relative response monitored by the calibration lamp after passages of the SAA for the shortest (red) and longest wavelength channels. The solid lines indicate the best fit lines of $R(t) = R_0[1 - A\exp(-t/\tau)]$ (see text). The bars at top indicate the SAA passage times.

Table 9. Uncertainty in the absolute surface brightness due to the present dark current estimate for one $8' \times 8'$ area of sky.

Channel Number	Uncertainty (MJy sr^{-1})	Channel Number	Uncertainty (MJy sr^{-1})	Channel Number	Uncertainty (MJy sr^{-1})	Channel Number	Uncertainty (MJy sr^{-1})
1	0.832	9	1.027	17	1.599	25	3.063
2	0.927	10	1.311	18	1.753	26	3.401
3	1.192	11	0.906	19	2.361	27	3.650
4	0.805	12	0.915	20	2.387	28	4.188
5	1.181	13	1.165	21	2.595	29	4.351
6	0.949	14	1.236	22	2.717	30	5.109
7	0.786	15	1.301	23	2.789	31	5.818
8	0.842	16	1.363	24	2.870	32	5.481

as the integrated signal. The area used for the background estimate on each side of a detection event was selected iteratively to provide the least noise in $(10-20) \times 1.024$s length data. The obtained integrated signals were converted into flux units with the conversion factors listed in Table 8. In the flux estimates, the events for which the signals of more than a half of the channels were less than the noises of the background (3σ) were removed from the list. In this process the quality of the signals of the event was also examined. About a half of the events were removed because of the quality criteria. The remaining 4605 detection events were processed further.

Whether the individual events correspond to the same object or not was examined based on the positional coincidence at first and then the correlation in the spectrum and flux level was examined. The association of each event was made iteratively. The final search rectangle area was $3'$ (in-scan) $\times 6'$ (cross-scan). The rms errors in the positional accuracy of the *MIRS* observations were estimated relative to the IRAS coordinate system to be about $1.5'$ (in-scan) and $2'$ (cross-scan). We had 2381 independent objects in the end. These include extended sources in addition to point sources.

Finally the fluxes of the events associated with the same object were co-added. Events with their fluxes deviating more than 30% from the average were removed from the co-add. Also in the averaging process, the channels with the large fluxes relative to the neighboring channels were marked as spikes. The noises of the averaged spectrum were calculated as a root mean square of the individual event noises and the scatter among the events. In most cases, the latter dominates in the flux uncertainty. Note that this uncertainty includes the uncertainty due to the location within the aperture.

6. COMPARISON WITH OTHER OBSERVATIONS

6.1. Point sources

Figure 7 shows some examples of comparison of the *MIRS* spectra with other observations for point sources. Since bright objects in the mid-infrared region are mostly variable stars, it is not very straightforward to make a direct comparison. Figure 7a shows the spectra of ω Cap taken by *MIRS* and the calibration template.[8] ω Cap is one of the bright standard stars used for the calibration of the *MIRS*. The difference thus indicates the uncertainty in the *MIRS* calibration. Figures 7b and c compare the *MIRS* spectra with those taken by ISO/SWS. The *MIRS* spectrum of DY Dra is in good agreement with the SWS spectrum, while that of U Cam shows an appreciable difference. Both stars are carbon stars and thus variables. Figure 7d plots the *MIRS* spectrum of X Hor with that of the IRAS LRS spectrum.

6.2. Diffuse emission

Figure 8 shows the comparison of the *MIRS* diffuse data with the COBE/DIRBE data in high Galactic latitude regions. The DIRBE data were extracted from the weekly averaged sky maps that had solar elongation angles

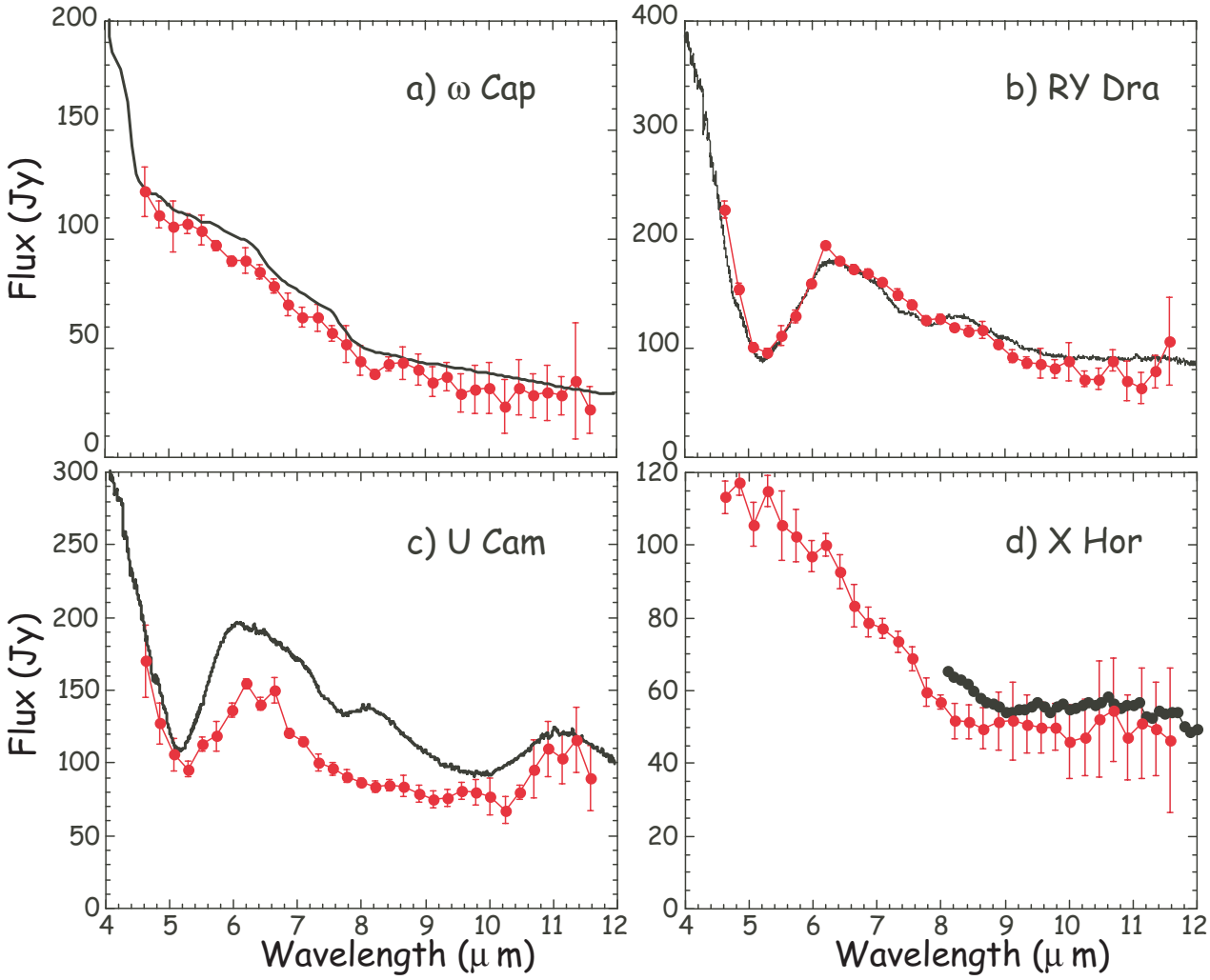

Figure 7. Comparison of the *MIRS* spectra with other observations. a) ω Cap, b) RY Dra, c) U Cam, and d) X Hor. Red lines with error bars indicate the *MIRS* spectra. Black lines indicate those by ISO/SWS (a, b, and c) or by IRAS LRS (d).

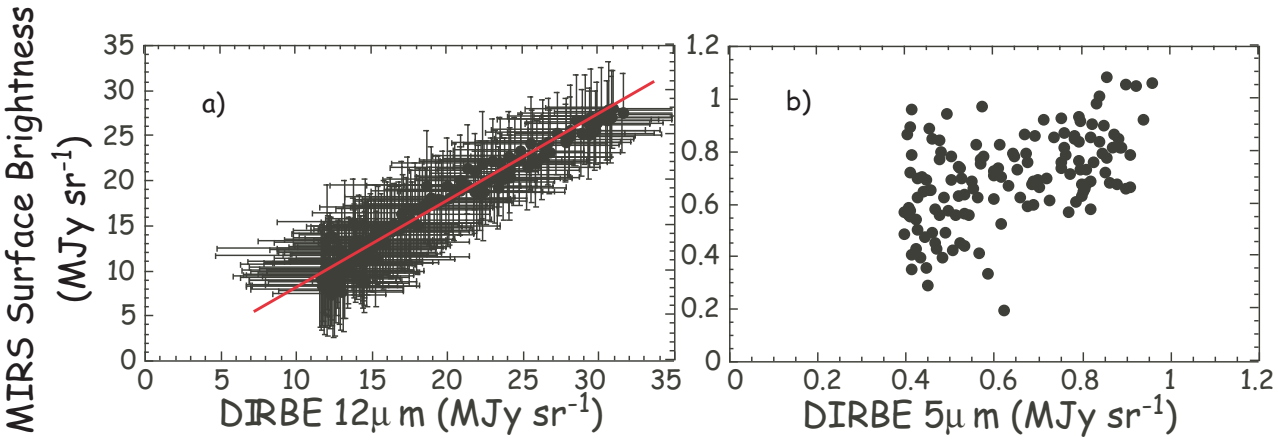

Figure 8. Comparison of the *MIRS* data with COBE/DIRBE intensity in high Galactic latitude regions. a) The average of #30–32 channels of the *MIRS* against DIRBE 12 μm. The solid line indicates the least-square fit result. b) The average of #2 and #3 of the *MIRS* against DIRBE 5 μm intensity. Error bars are large and not shown.

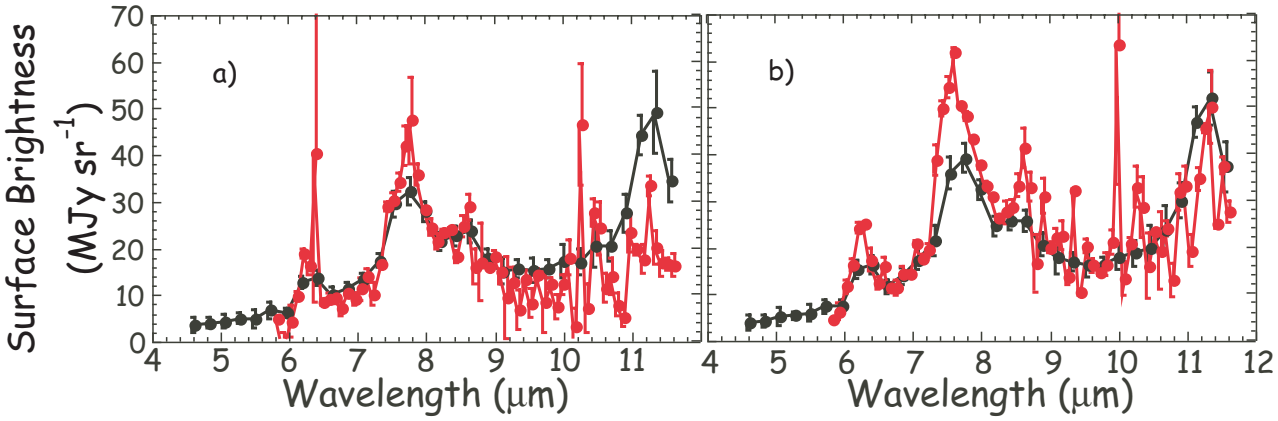

Figure 9. Comparison of the *MIRS* spectra (black lines) with PHT-S spectra (red lines) for the diffuse Galactic radiation at two positions near the Galactic plane: a) at $(l,\, b) = (50.^\circ74, 0.^\circ59)$ and b) $(l,\, b) = (51.^\circ09, -0.^\circ04)$.

and an observation season close to the *IRTS* observations. The *MIRS* data were averaged over the corresponding DIRBE field of view (0.°7). Figure 8a indicates the plot of the average of the surface brightness of *MIRS* channel 30–32 against the COBE/DIRBE 12 μm surface brightness. A least-squares fit gives [MIRS intensity (MJy sr^{-1})] $= (0.96 \pm 0.02)$[DIRBE 12 μm] $-(1.6 \pm 0.33)$. Taking account of the fact that the DIRBE spectral band went longer than 12 μm and the DIRBE aperture was much larger than that of the *MIRS*, the agreement is good. The difference in the zero level is within the estimated accuracy (Table 9). Figure 8b shows a comparison of the average of *MIRS* channels 2 and 3 with the DIRBE 5 μm intensity. Because of the low sky brightness at 5 μm, the plot shows a large scatter, but the agreement is reasonable.

Figure 9 shows a comparison of the *MIRS* spectra with those taken by ISO/PHT-S at two positions in the W51 region. Although the *MIRS* data were extracted from positions the same as those of the PHT-S observations, the difference in the size of the aperture (PHT-S has a 24″ square aperture) makes direct comparison difficult. At the first position the PHT-S intensity is fainter in the longer wavelengths, while it is larger around the 7.7 μm at the second position. Possible small-scale variations may account for the difference. Taking account of the difference in the aperture size, the *MIRS* spectra are in fair agreement with the PHT-S data.

7. DATA PRODUCTS

The presently available data product of the *MIRS* observations is the *MIRS* Point Source Catalog (MIRSPSC). It contains the mid-infrared spectra of 536 sources. It consists of the list of the sources MIRSPSC.dat and the spectra of the sources MIRSName.spa, where MIRSName is the name of the source in the source list (R.A. and Dec. of the source position). The format of these files is shown Table 10. The point source extraction process is described in section 5. The MIRSName is defined based on the *MIRS* detection position (B1950) to allow direct comparison with the IRAS names. The *MIRS* position is, however, given in the J2000.0 coordinates. The quality flag is defined based on the number of channels that have 'good' data. The quality of the data of each channel is evaluated as 'bad' if the signal is negative, not available because of errors in the data processing, or associated with a large uncertainty (> 0.025 mV s^{-1} or S/N < 3) or large background noise. Otherwise it is defined as 'good'. The quality flag is defined as 0 (bad) if $N_b > 6$, 1 if $6 \geq N_b > 4$ or $4 \geq N_b > 2$ and the average S/N is less than 3, 2 if $4 \geq N_b > 2$ or the average S/N is less than 3, and 3 (good) otherwise, where N_b is the number of 'bad' channels. Associations with IRAS sources (NI) were searched for within a circle of $8'$ radius. The first 11 lines of MIRSName.spa contain a digest of the information in the MIRSSPC.dat. The parameter SPK in the spectrum file (MIRSName.spa) indicates the information on the despiking corrections applied to the spectrum, defined as 0 if no despiking was applied, 1 if despiking was applied, -1 if the data were not reliable, and -2 if the flux could not be determined.

The dataset of the diffuse emission is yet to be released. They will consist of the FITS files of each channel of the observed sky. The time sequential data (BDM and DIF) are also planned to be released in the future.

Acknowledgement

We thank all the members of the *IRTS* team for their continuous help and encouragement and the SFU project team for their help in the *IRTS* observations. The pointing reconstruction of the *IRTS* observations was carried out by IPAC. We thank them for their efficient help.

REFERENCES

1. Murakami, H. et al. 1994, ApJ, 428, 354
2. Murakami, H. et al. 1996, PASJ, 48, L41
3. Roellig, T. L., Onaka, T., McMahon, T. J., & Tanabé, T. 1994, ApJ, 428, 370
4. Onaka, T. 1995, Appl. Opt., 34, 659
5. Roellig, T. L., Mochizuki, K., Onaka, T., Tanabé, T., Yamamura, I., & Yuen, L. 1996, Proc. of SPIE, 2817, 258
6. Onaka, T., Ishihara, D., Ootsubo, T., Chan, K.-W., Yamamura, I., Murakami, H., Tanabé, T., Roellig, T. L., & Cohen, M. 2002, ESA SP-481, in press
7. Lange, A. E., Freund, M. M., Sato, S., Hirao, T., Matsumoto, T., & Watabe, T. 1994, ApJ, 428, 384
8. Cohen, M., Walker, R. G., Carter, B., Hammersley, P., Kidger, M,, & Noguchi, K. 1999, AJ, 117, 1864
9. Witteborn, F. C., Cohen, M., Bregman, J. D., Wooden, D. H., Heere, K., & Shirley, E. L. 1999, AJ, 117, 2552
10. Cohen, M., Witteborn, F. C., Roush, T., Bregman, J., & Wooden, D., 1998, AJ, 1671
11. Yamamura, I. & the IRTS Team 1997, in Proc. of the Diffuse Infrared Radiation and the IRTS, eds. H. Okuda, T. Matsumoto, & T. L. Roellig, A.S.P. Conf. Ser. 124, 72
12. Yamamura, I., Onaka, T., Tanabé, T., Roellig, T. L., & Yuen, L. 1996, PASJ, 48, L65

Table 10. Format of the *MIRS* point source catalog dataset

MIRS Point Source Catalog List (MIRSPSC.dat)

Start Byte	Format	Name	Description
The first line contains the header information.			
1	10A	MIRS Name	R.A. (5 bytes) and Dec (5 bytes) of the MIRS position
11	1A	blank	
12	16A	Position	*MIRS* position in format of `01h23.4m +56d78'` (J2000.0)
28	2F6.1	l and b	Galactic coordinates in degree
40	I3	ND	Number of events used for the co-add
43	1A	blank	
44	1A	C	Spectral classification[12]
45	1A	blank	
46	1A	A	Positional accuracy. g: $< 2'$, m: $< 5'$, and b:$< 30'$
47	F8.2	`F_b1`	Average flux of channels 1 to 8 in Jy
55	F8.2	`F_b2`	Average flux of channels 9 to 16 in Jy
63	F8.2	`F_b3`	Average flux of channels 17 to 24 in Jy
71	F8.2	`F_b4`	Average flux of channels 25 to 32 in Jy
79	1B	blank	
80	4I1	Quality flag	One for each band (`F_b*`). 3: good, 2: O.K. 1: inaccurate (see text)
84	I2	NI	Number of nearby IRAS sources brighter than 5Jy at 12 μm within $8'$.
86	1	blank	
87	10A	IRAS Name	
97	F7.1	`F12`	12 μm IRAS flux in Jy
104	F6.2	DR	Distance to the brightest nearby IRAS source in arcminute.
110	A3	LRS	IRAS LRS index

MIRS Point Source Spectrum File (MIRSName.spa)

The first eleven lines contain the MIRS PSC information	
Line	Content
1	Catalog name, version, and creation date and time
2	Blank line
3	Description of line 4
4	MIRS Name, Positions Number, ND, C, A
5	Blank line
6	Description of line 7
7	Four average fluxes and quality flag
8	Blank line
9	Description of line 10
10	IRAS Name, 12 μm IRAS flux, dr, LRS
11	Blank line

Lines 12 and 13 contain the column information after line 14. From line 14 the following data are stored per line.

Start Byte	Format	Name	Description and unit
1	F8.3	λ	Wavelength in μm.
9	E11.3	F	Flux in Jy
20	E11.3	E	Uncertainty in flux in Jy
33	E11.3	B	Background flux in Jy per beam
44	E11.3	BE	Uncertainty in background flux in per beam
55	I3	SPK	Information of despiking (see text)